Newsletters on Stratigraphy, Vol. 00/0 (0000), 000–000 **Early Access Article**
Published online July 2025

Planktonic foraminiferal and isotope stratigraphy of the upper Cenomanian-Turonian interval in the Zagros Basin, SW Iran

Yadolah Ezampanah[1,*], Behnaz Kalanat[2], Ahmad Reza Karimi[3], Hassan Mohseni[1], Stefano Fasone[4] and Giovanna Scopelliti[4]

With 10 figures

Abstract. A high-resolution bio- and chemostratigraphic study based on planktonic foraminifera and carbon stable isotope of the late Cenomanian–late Turonian time interval of the Sarvak Formation was undertaken in the Zagros Basin (SW Iran). In this research, a hemipelagic succession, named the Tang-e Bawlek section, was inspected. Significant documented bio-events in stratigraphic order include lowest occurrence (LO) of *Praeglobotruncana algeriana*, the highest occurrences (HO) of *Thalmanninella appenninica*, *Th. deeckei*, *Rotalipora montsalvensis*, *Th. greenhornensis* and *R. cushmani*, LO of *Helvetoglobotruncana praehelvetica*, HO of *La. bentonensis*, "*Heterohelix*" shift, LO of *Helvetoglobotruncana helvetica* and finally HO of *H. helvetica*. These bio-events have led to the recognition of four biozones (from *Rotalipora cushmani* Zone to *Dicarinella primitiva-Marginotruncana sigali* Zone) from the Tethyan realm. Integrating of the well-documented bio-events with a high-resolution $\delta^{13}C$ curve, particularly around the Cenomanian/Turonian boundary (CTB), enabled comprehensive documentation of OAE2 and its three distinct associated peaks (a, b and c) as well as facilitated correlation with key reference curves. These results reveal that in contrast to the other parts of the Zagros Basin, where the CTB is represented by a marked disconformity or sea level fall, this portion of the Lurestan Subzone exhibits evidence of deep marine conditions. However, the detailed lithological and microfacies observations point to the development of a condensed horizon with a low sedimentation rate, rich in glauconite and phosphate located just above the peak c of the $\delta^{13}C$ curve, which can be associated with a short hiatus close to the CTB. Palaeoecological reconstructions of the studied interval revealed three major changes in the depositional conditions, establishing a notable eutrophic condition during the OAE2 interval accompanied by a well-developed oxygen minimum zone (OMZ).

Keywords. Biostratigraphy; Stable isotopes; OAE2; Sarvak Formation; Cenomanian/Turonian boundary; Palaeoenvironments

1. Introduction

The Early to middle Cretaceous time interval is characterized by different oceanic anoxic events (OAEs) in the Earth's history. Among these OAEs the CTBE, also known as OAE2 or Bonarelli event (Schlanger & Jenkyns 1976, Schlanger et al. 1987), is the most pronounced and intensively studied worldwide. The OAE2 is a short–lived event (100 and 900 kyr Caron et al. 1999, ~ 400 kyr Scopelliti et al. 2004, 563–601

Author's addresses:
[1] Department of Geology, Faculty of Science, Bu-Ali Sina University, Hamedan, Iran
[2] Department of Palaeobotany, Research Institute of Forests and Rangelands, Agricultural Research, Education and Extension Organization (AREEO), Tehran, Iran
[3] Geology Department, Earth Sciences Faculty, Shahid Chamran University, Ahvaz
[4] Dipartimento di Scienze della Terra e del Mare (DiSTeM), Università di Palermo, Via Archirafi 36, 90123 Palermo, Italy
[*] Corresponding author: y.ezampanah@basu.ac.ir

 www.borntraeger-cramer.de
DOI: 10.1127/nos/2025/0855 0078-0421/2025/0855 $ 00.00

kyr Sageman et al. 2006, 430–445 kyr, Voigt et al. 2008, 820 ± 25 kyr, Li et al. 2017, 930 ± 25 kyr Gangl et al. 2019) characterized by the massive eruptions of submarine volcanisms (Larson 1991, Leckie et al. 2002, Snow & Duncan 2005, Ernst & Youbi, 2017, Schröder-Adams et al. 2019), maximum global warmth of the Cretaceous (e.g., Fletcher et al. 2008, Barclay et al. 2010), and widespread organic-rich black shale deposition (e.g., Kuhnt et al. 1990, Kuypers et al. 2002, Pancost et al. 2004, Falzoni & Petrizzo 2022). Literatures confirm the synchronicity of some planktonic foraminiferal bio-events at the CTB (e.g. Falzoni et al. 2018, Falzoni & Petrizzo 2020, Salhi et al. 2022) and their integration with the $\delta^{13}C$ isotope stratigraphy is regarded as a robust stratigraphic tool for global correlation among different sedimentary basins (Jarvis et al. 2006; Wendler et al. 2009; Voigt et al. 2010, 2012; Razmjooei et al. 2018; Navidtalab et al. 2019; Kalanat & Vaziri-Moghaddam 2019).

In the Zagros fold and thrust belt (ZFTB) in SW Iran, the CTB occurs within the Sarvak Formation. This formation received lots of attention due to acting as one of the most prolific hydrocarbon reservoirs in the Middle East and the world, representing lateral and vertical facies variations and yielding high faunal richness and diversity (Wynd 1965, Motiei 2003, Kalanat & Vaziri-Moghaddam 2019, Mohseni & Zeybaram Javanmard 2020, Vaziri-Moghaddam & Kalanat 2020).

Previous researches indicate that the sedimentary record across the CTB varies significantly within differnt parts of the ZFTB, ranging from continuous sedimentation to sequences interrupted by short hiatuses or regional unconformities (Alavi 2004; Ghasemi-Nejad et al. 2006; Taghavi et al. 2006; Razin et al. 2010; Rahimpour-Bonab et al. 2012; Hajikazemi et al. 2010, 2012; Navidtalab et al. 2019; Kalanat & Vaziri-Moghaddam 2019; Mohseni & Zeybaram Javanmard 2020; Ezampanah et al. 2022; Bagherpour et al. 2023; Esfandyari et al. 2023). Continuous and transitional deposition across the CTB in the offshore Cham-e-Zeytoon section (Fars Subzone) is supported by the integration of planktonic foraminifera biostratigraphy, carbon isotope stratigraphy, field and facies analysis (Bagherpour et al. 2023). In the Kabir Kuh and Chenareh anticlines (Lurestan Subzone), a less pronounced positive $\delta^{13}C$ excursion linked to OAE2 coupled with sharp lithological variations reveals an incomplete CTB sequence, possibly due to a local hiatus (Navidtalab et al. 2019, Asadi Mehmandosti et al. 2021). In the Lar Anticline a temporary shift to inner neritic facies lacking planktonic foraminifera, indicative of a sea level fall in the earliest Turonian, corresponds to the regional unconformity (Kalanat & Vaziri-Moghaddam 2019).

While the biostratigraphy, microfacies, depositional environments, and sequence stratigraphy of the Sarvak Formation are well defined, the integration of biostratigraphy with carbon-isotope stratigraphy remains limited, with the exception of studies conducted by Navidtalab et al. (2019), Kalanat & Vaziri-Moghaddam (2019) and Bagherpour et al. (2023). Furthermore, the documentation regarding the paleoecological aspects of this formation, are still scarse compared to its counterparts in the western Tethys Ocean.

The main scope of the present research is to establish a zonal framework for the inspected interval of the Sarvak Formation using planktonic foraminifera. Our biostratigraphic data are backed up by new high-resolution carbon isotope data calibrated to other reference curves. Quantitative data for the Cenomanian/Turonian planktonic foraminiferal assemblages in the studied section are also provided to interpret the turnover of these taxa during the OAE2 interval.

2. Geological setting

The middle Cretaceous along the eastern margin of Arabian Plate (Fig. 1A) is characterized by a dramatic event that marks a change from a tectonically stable passive margin into an active compressional setting as a consequence of initial closure of the Neotethys Ocean (Glennie 2000; Ziegler 2001; Sharland et al. 2001; Hollis & Sharp 2011; Piryaei et al. 2010, 2011). This tectonic evolution has triggered the reactivation of deep-seated basement normal faults, salt domes and emergingmultiple paleohighs surrounded by intrashelf basins (e.g., the Garau Basin) in the ZFTB and elsewhere in the Middle East (Sharland et al. 2001; van Buchem et al. 2002; Sepehr & Cosgrove 2004, 2005; Alavi 2004, 2007; Leturmy & Robin 2010; Bromhead et al. 2022). This tectonic evolution also had a profound impact on the facies changes and depositional environments of the Sarvak Formation. The ZFTB from the NW to the SE, has been structurally divided into several tectonic subzones including Lurestan, Izeh, Dezful, and Fars (Fig. 1B–C). The Sarvak Formation comprises two distinct carbonate facies types: the neritic cliff-forming carbonate predominantly composed of rudist and other benthic fauna and the basinal hemipelagic facies mainly composed of planktonic foraminifera, ammonites, and calcispheres

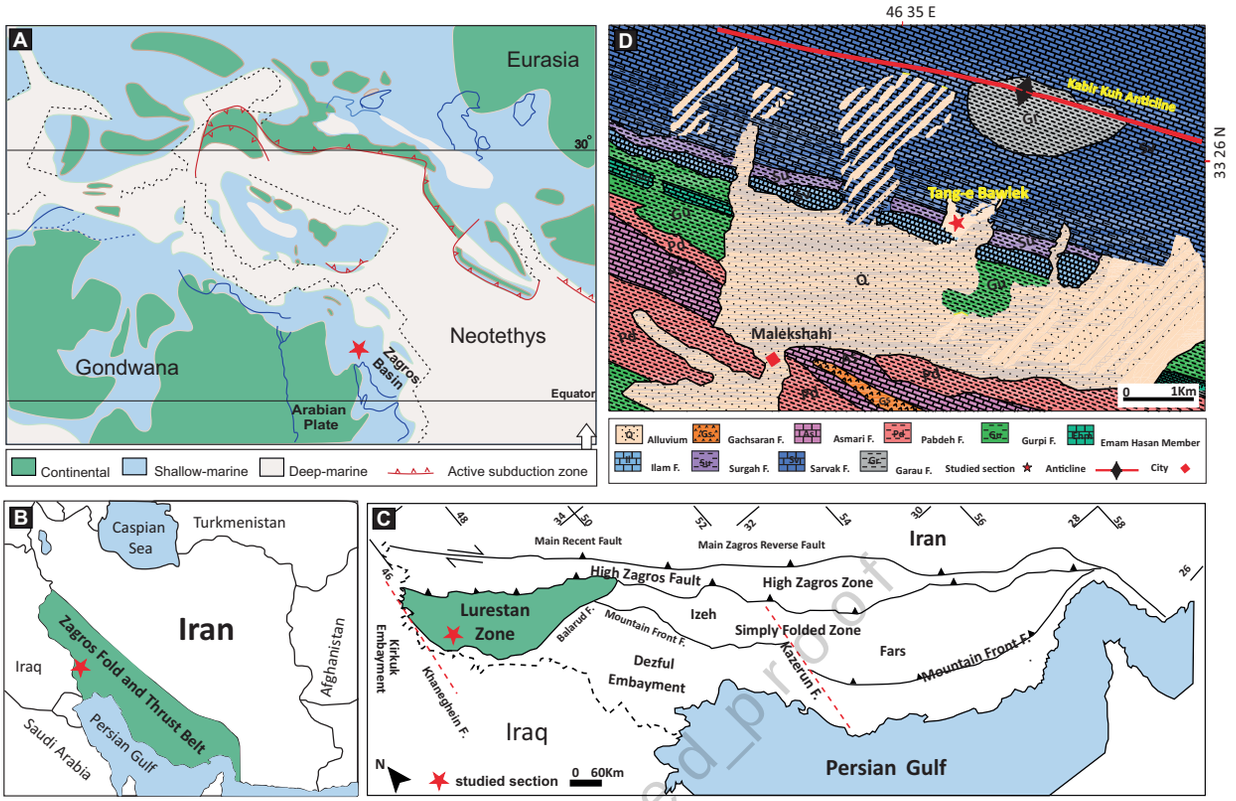

Fig. 1. A. Late Cenomanian paleogeography around the Neo-Tethys Ocean with approximate position of the ZFTB (after Barrier and Vrielynck 2008), **B–C.** Structural map of the ZFTB (modified after Farzipour-Saein et al. 2009), and **D.** Geological map of the study area in which the location of the measured sections is shown (modified after Mohseni & Zeybaram Javanmard 2020).

(James & Wynd 1965, Setudehnia 1978, Motiei 2003, Ghabeishavi et al. 2010). Three unconformities including middle Cenomanian, late Cenomanian–early Turonian, and mid-Turonian were identified in the neritic facies (Sharland et al. 2001, Razin et al. 2010, Navidtalab et al. 2016, Mehrabi et al. 2022). The second one, out of the three mentioned, was identified across most parts of the ZFTB with evidences of significant subaerial exposure, erosion, and extensive meteoric diagenesis (Sharland et al. 2001; Razin et al. 2010; Hollis 2011; Rahimpour-Bonab et al. 2012, 2013; Bagherpour et al. 2021). The Lurestan Subzone exhibits significant sedimentary thickness and facies variations compared to other simply folded belt subzones. From the Early to Late Cretaceous the sedimentary succession in this subzone was dominated by deep marine facies (James & Wynd 1965, Ezampanah et al. 2013, Sarfi et al. 2015), which transition laterally into neritic carbonates toward the Dezful Embayment and Fars Subzone (James & Wynd 1965).

3. Material and methods

3.1. Studied section

The study area is located in the simply folded belt, the Lurestan Subzone, at the Kabir Kuh Anticline (Fig 1D). The current research focuses on the hemipelagic unit of the Sarvak Formation in the Tang-e Bawlek section, about 4 km to the northeast of the Malekshahi city at 33°25’02.8” N, 46°30’34.03” E (Fig. 1C-D). This section presents a spectacular exposure of deep marine late Albian through Coniacian succession.

This section (56 m thick) was lithostratigraphically described, bed by bed, and sampled for micropaleontological and geochemical studies, with a sampling interval of 0.05 m to 0.1 m (at the C/TB) and 0.5 to 1 m for the rest of the section (Fig. 2). The lower 11 m of the section is dominated by medium to thick-bedded grey to cream limestones containing rare ammonites, alternating with thin-bedded grey argillaceous limestones. Upward the section, there is 13.3 m alter-

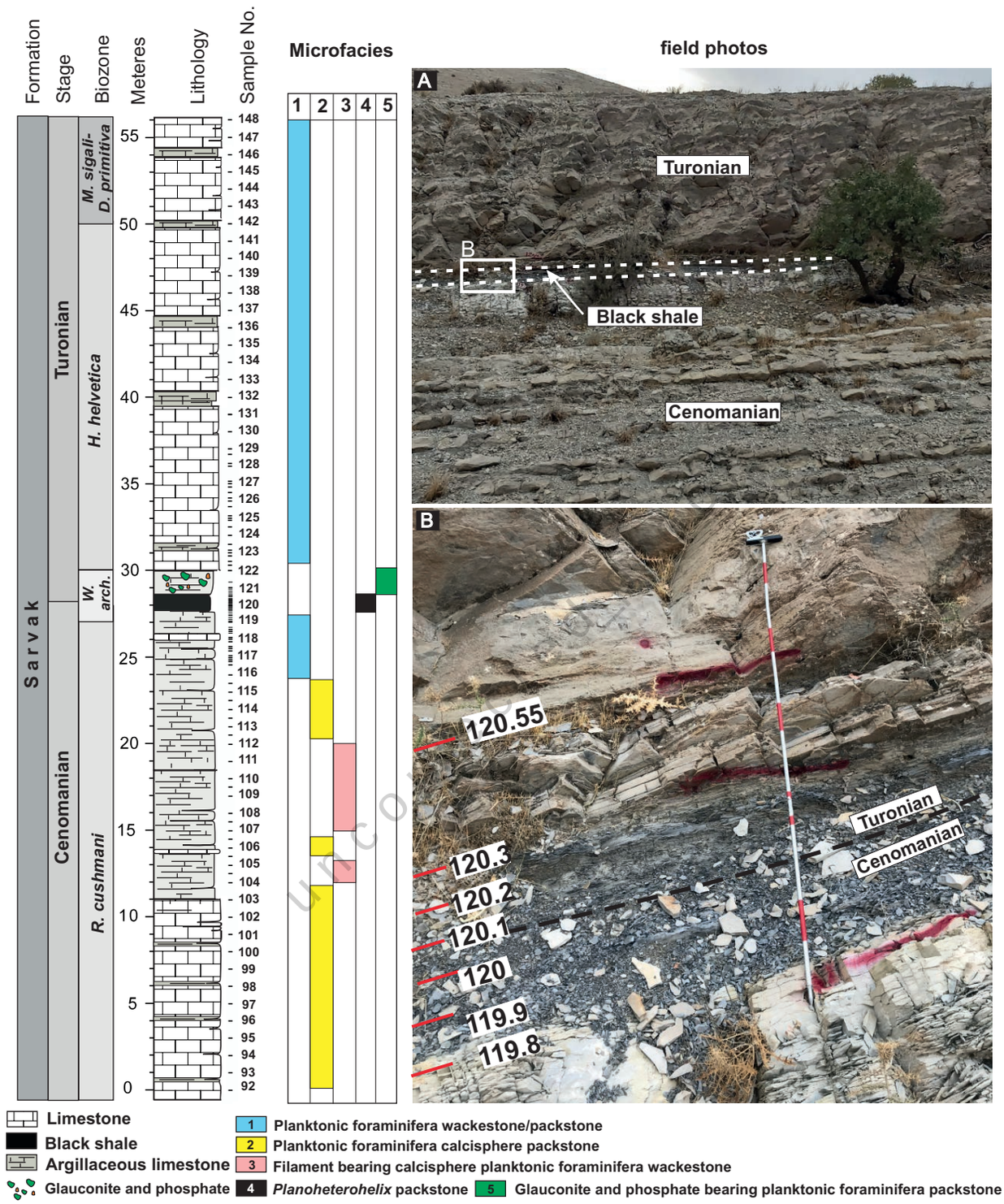

Fig. 2. Lithostratigraphic log and identified microfacies of the pelagic part of the Sarvak Formation in the Tang-e Bawlek section, **A.** Field photograph of the study section. The black shale layer approximately indicates the CTB in this interval, **B.** Close-up view of black shale bed across the CTB. The exact location of the CTB is based on peak c in the $\delta^{13}C$ profile (see text).

nation of thin to medium-bedded grey argillaceous limestones and grey to dark grey shales. The next interval with 4.70 m thick (from 24.30 m to 29 m) which approximately includes the CTB, can be categorized in the following units (Fig. 2A–B): the first unit (from 24.30 m to 26.45 m) is characterized by alternating laminated to thin-bedded dark grey to black fissile shales and thin to medium-bedded dark grey to black argillaceous limestones. The overlying unit with 1.35 m thickness (from 26.45 m to 27.80 m) comprises thin to medium-bedded dark grey to grey argillaceous limestones. The third unit (from 27.80 m to 28.34 m), encompassing the Cenomanian/Turonian stage boundaries, is represented by laminated black shales. This unit is underlined by 15 cm thin-bedded dark grey argillaceous limestone, followed by 5 cm laminated dark gray to black shales. Finally, the 27.46 m-thick interval at the uppermost part of the studied section is dominated by thin to medium-bedded cream to grey limestones alternating with thin to medium-bedded grey argillaceous limestones.

3.2. Foraminifera

Taxonomic uncertainties, varying species definitions, misidentifications, issues with sampling resolution and processing, rare occurrences of marker species, and poor fossil preservation all contribute to the diachronous records related to the lowest and highest occurrence of biostratigraphic index taxa among Cretaceous planktonic foraminifera (Desmares et al. 2007, Petrizzo et al. 2011, Wendler 2013, Huber & Petrizzo 2014, Bidgood & Simmons 2023). Analyzing planktonic foraminifera within a succession of variable lithologies (shales, argillaceous limestones, and limestones) using a single method, such as washing, might be inadequate. Washing the limestones via acetic acid to isolate foraminiferal content could potentially dissolve some of the index taxa. Hence, to comprehensively document all significant planktonic foraminiferal bio-events for establishing a reliable biozonation framework throughout the CTB, we employed a combination of washing and thin section methods for almost all samples. A total of 30 washed samples and 72 thin sections have been prepared. For the washing process, approximately 100 g of indurated limestones, shales and argillaceous limestones were crushed into smaller fragments (mostly 2–5 mm) and subsequently placed into 500 ml glass beakers. These samples were then subjected to various concentrations of acetic acid and distilled water (100 ml of 80% and 60% acetic acid) over a time span that varied from 30 minutes up to 8 hours following the methodologies established by Kariminia (2004), Malik et al. (2022) and Ištuk et al. (2023). By forming a thick foam with no evidence of effervescence, the samples were washed over 120 and 63 μm sieves and dried to obtain washed residues. Planktonic foraminifera were plentiful in most of the samples, with a single pick being sufficient to achieve the required quantity for qualitative and quantitative analyses. Counting was done only on washed residues, and thin sections were used here better to position the LO and the HO of important taxa. The preservation rate was generally poor to moderate in the limestones and moderate to good in the shales and argillaceous limestone intervals. Diversity of planktonic foraminifera was calculated by species richness and by applying the Shannon-Wiener diversity index:

$$H(S) = -\sum_{i=1}^{s} Pi \times \ln Pi$$

Where, S is number of species and Pi the proportion of ith species (Murray 1991). The relative abundances of planktonic foraminiferal species in the studied interval are reported in Supplementary Table S1. The identification of planktonic foraminifera species and zonal schemes is in agreement with those of Premoli Silva and Verga (2004), Petrizzo & Huber (2006), Ando & Huber (2007), Caron & Premoli Silva (2007), González-Donoso et al. (2007), Coccioni & Premoli Silva (2015), Haynes et al. (2015), Petrizzo et al. (2015), Petrizzo & Gilardoni (2020), Huber et al. (2022) and the mikrotax online database at https://www.mikrotax.org/pforams/index.html for Mesozoic planktonic foraminifera (Huber et al. 2016). The sedimentation rate was calculated based on the age of zonal markers (LO of *P. algeriana*, HO of *R. cushmani*, and LO of *H. helvetica*) in two intervals. The ages of bio-events are from Falzoni et al. (2018) (Supplementary Table S2).

All the samples are stored at the palaeontology laboratory of the Bu-Ali Sina University, Iran.

3.3. Stable carbon and oxygen isotopes and carbonate content determination

Carbon and oxygen isotope compositions were measured on powdered bulk samples (123 samples) in the laboratory of DiSTeM, University of Palermo. Prior to powdering, the samples were carefully examined: the micritic matrix was preferentially sampled, while areas

of high carbonate cements and veins were avoided. The CO_2 gas was obtained by the classical phosphoric acid–calcium carbonate reaction method using an automated Carbonate Preparation Device (Thermo Scientific GasBench II). The carbon and oxygen stable isotope compositions were measured with a Thermo Scientific Delta V Advantage continuous flow isotope ratio mass spectrometer. The results are expressed in delta (δ‰) notations relative to the V-PDB standard. Every 10 samples, an internal laboratory standard (Carrara Marble with $\delta^{18}O_{V\text{-}PDB}$ = -2.43‰ and $\delta^{13}C_{V\text{-}PDB}$ = 2.43‰) was run and the NBS19 international standard ($\delta^{18}O_{V\text{-}PDB}$ = -2.20‰ and $\delta^{13}C_{V\text{-}PDB}$ = 1.95‰) was also measured every 20 samples. Precision for duplicate analyses was better than 0.1‰ for carbon and oxygen. Moreover, the carbonate content of 68 selected samples (from 111 to 130) around the CTB, was determined by a Micro-calcimeter, equipped with a pressure gauge, based on the gas volumetric method. The $CaCO_3$ percentage was estimated from the CO_2 released by the reaction of the powdered bulk samples with hydrochloric acid 8N

4. Results

4.1. Microfacies

The deep marine argillaceous limestones and limestones of the hemipelagic part of the Sarvak Formation in the Tang-e Bawlek section are rich in planktonic foraminifera and pithonellids. Subordinate bioclasts include small benthic foraminifera, thin filaments and sponge spicules (Fig. 3A–F).

According to the faunal assemblages and depositional textures, 5 microfacies were recognized within the CTB interval (Figs. 2 and 3A-F). These microfacies are as follow: 1) Planktonic foraminifera wackestone/packstone (Fig. 3A): both keeled and non-keeled morphotypes are the principle components of this microfacies, 2) Planktonic foraminifera calcisphere packstone (Fig. 3B) in which calcispheres, non-keeled planktic foraminifera and to a lesser extent rotaliporids are the dominant constituents, 3) Filament bearing calcisphere, planktonic foraminifera wackestone (Fig. 3C), 4) *Planoheterohelix* packstone (Fig. 3D): mainly dominated by biserial planktonic foraminifera (especially *Planoheterohelix*). Subordinate biota include radially elongated chambers (*Clavihedbergella simplex*), whiteinellids, and rare specimens of *Pithonella ovalis*, and 5) Planktonic foraminifera packstone rich in glauconite, phosphate and pyrite (Fig. 3E–F).

4.2. Planktonic foraminiferal biozonations

In the studied interval of the Sarvak Formation, 48 species belonging to 17 genera of planktonic foraminifera were recognized. The stratigraphic distribution and abundances of the identified species are illustrated in Figure 4. Based on the LO and HO of the index planktonic foraminiferal species, the studied interval is assigned to the stratigraphic interval from the late Cenomanian *R. cushmani* Zone to the late Turonian *Dicarinella primitiva-Marginotruncana sigali* Zone. Figures 5 and 6 show the main planktonic foraminiferal species in the studied interval. A brief description of the recognized zones is being summarized as below:

The presence of *Rotalipora cushmani* at the base of the studied interval (sample 92, Figs. 4 and 7) points to the late middle to latest Cenomanian *R. cushmani* Total Range Zone (Coccioni and Premoli Silva 2015). In particular, the association of *Whiteinella aprica*, *W. paradubia*, *W. brittonensis* and *W. archaeocretacea* at the base of the studied interval would suggest an age no older than early late to latest Cenomanian, which can be assigned to the upper part of the *R. cushmani* Zone, corresponding to the *P. algeriana* Subzone with early late to latest Cenomanian age (Coccioni & Premoli Silva 2015). This subzone is defined as an interval from the LO of the mentioned taxon (*P. algeriana*) to the HO of *R. cushmani*. The LO of *P. algeriana* (sample 94 at 2 m, Fig. 4), is known to occur in the mid-upper part of *R. cushmani* Zone (Premoli Silva & Verga 2004, Coccioni & Premoli Silva 2015, Falzoni et al. 2018). Important planktonic foraminiferal bio-events in this interval, in stratigraphic order, are the LO of *P. algeriana* close to the beginning of the zone; HOs of *Thalmanninella appenninica* and *Schackoina bicornis* in the middle part of the zone (sample 105 at 13 m); 3); HOs of *Clavihedbergella simplicissima*, *Th. deeckei*, and *R. montsalvensis* (sample 117 at 25 m), the HO of *Th. greenhornensis* (sample 118 at 26 m) and the HOs *R. cushmani*, and *C. amabilis* (sample 119 at 27 m). *Helvetoglobotruncana praehelvetica*, which is regarded as the precursor to *H. helvetica* (Huber & Petrizzo 2014, Petrizzo et al. 2021), also makes its LO at sample 119 (Fig. 4). *Muricohedbergella delrioensis*, *M. planispira*, *Planoheterohelix reussi* and *P. moremani* are the dominant species in this zone (Fig. 7). This biozone also exhibits a notable bloom of pithonellids (*Bonetocardiella*

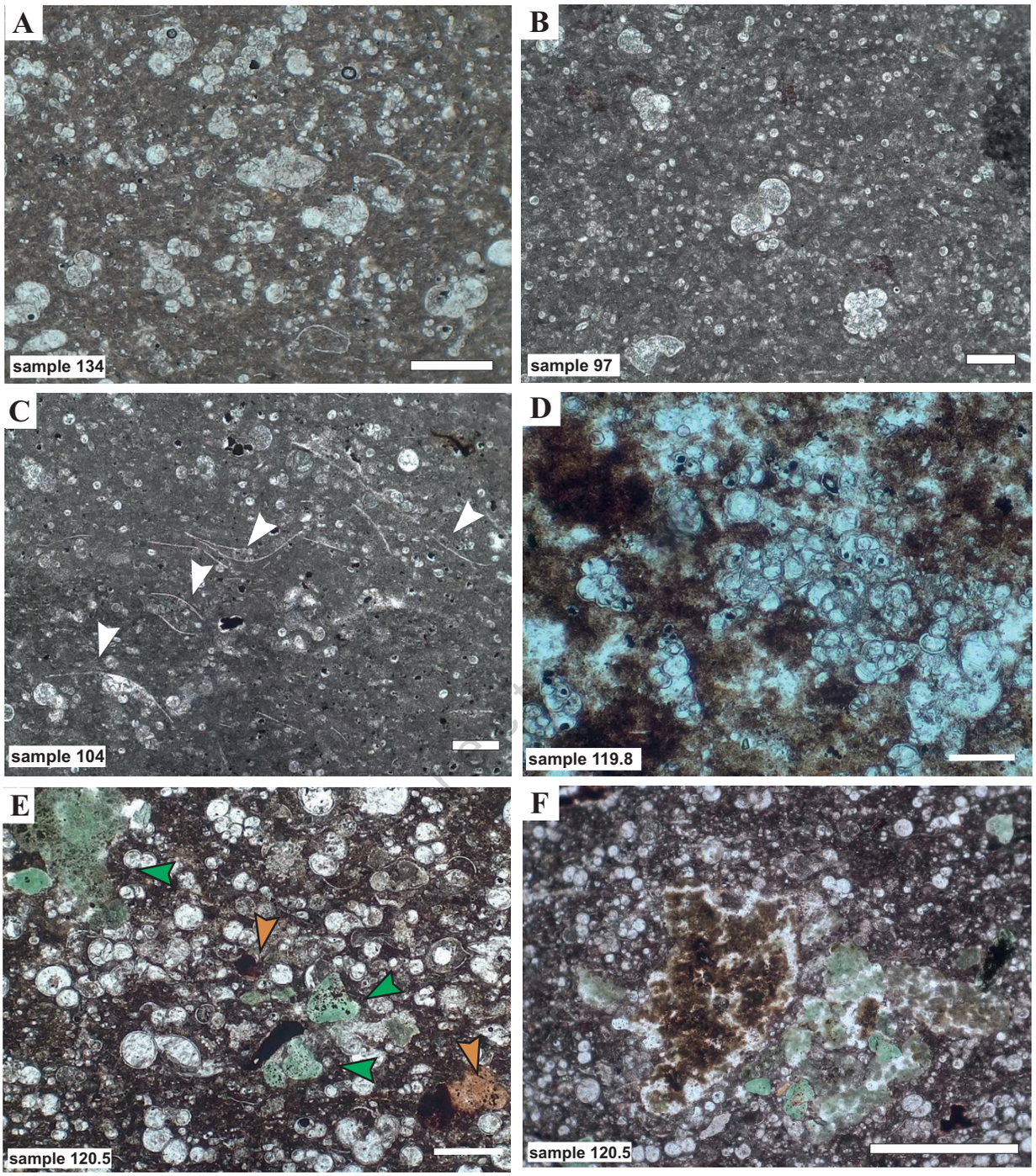

Fig. 3. Common microfacies in the CTB interval of the Tang-e Bawlek section. **A**. Planktonic foraminifera wackestone/packstone, **B.** Planktonic foraminifera calcisphere packstone, **C**. Filament (white arrows) bearing calcisphere planktonic foraminifera wackestone, **D.** *Planoheterohelix* packstone, and **E–F.** Glauconite and phosphate grains (green and orange arrows, respectively) observed in thin sections at the CTB. Scale bars A-B equal 500 µm and C-D equal 100 µm.

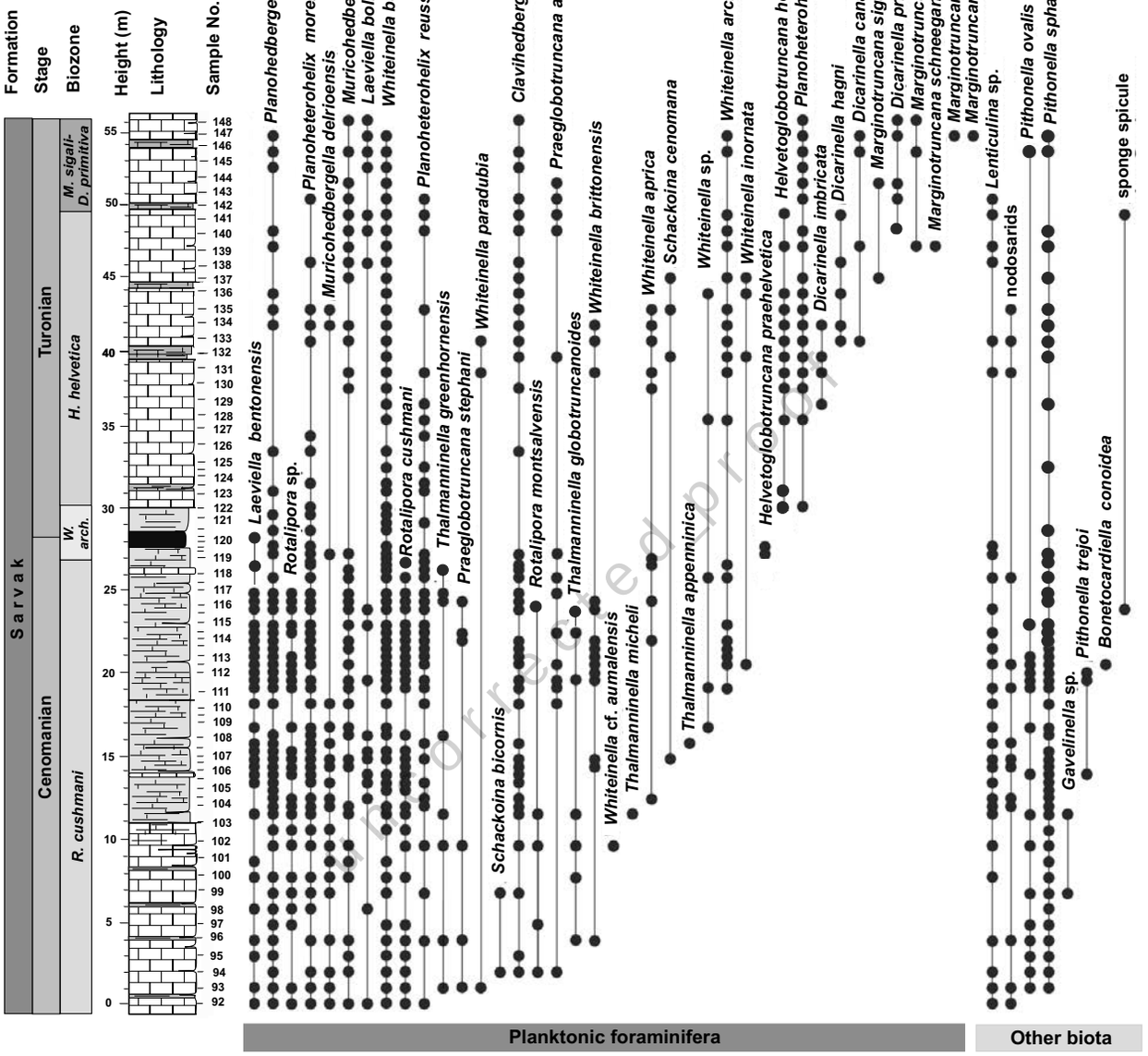

Fig. 4. Planktonic foraminifera distribution and biozones and associated biota of the upper Cenomanian to upper Turonian succession of the Tang-e Bawlek section. Abbreviations, *W. archa.*: *Whiteinella archaeocretacea* Zone.

Fig. 5. **A–B.** *Clavihedbergella simplex* (Morrow), samples 127 and 135, **C**. *Whiteinella paradubia* (Sigal), sample 117.5, **D–E.** *Laeviella bentonensis* (Morrow), samples 112.5 and 117, **F.** *Planohedbergella ultramicra* Subbotina), sample 117.5, **G.** *Whiteinella baltica* Douglas and Rankin, sample 141, **H.** *Praeglobotruncana delrioensis* (Plummer), sample 113.5, **I.** *Muricohedbergella planispira* (Tappan), sample 135, **J.** *W. brittonensis* (Loeblich and Tappan), sample 114, **K.** *Helvetoglobotruncana praehelvetica* (Trujillo), sample 120.5, **L–M.** *Dicarinella imbricata* (Mornod), samples 130 and 132, **N–O.** *Praeglobotruncana algeriana* Caron, samples 94, 141. Scale bars equal 100 µm.

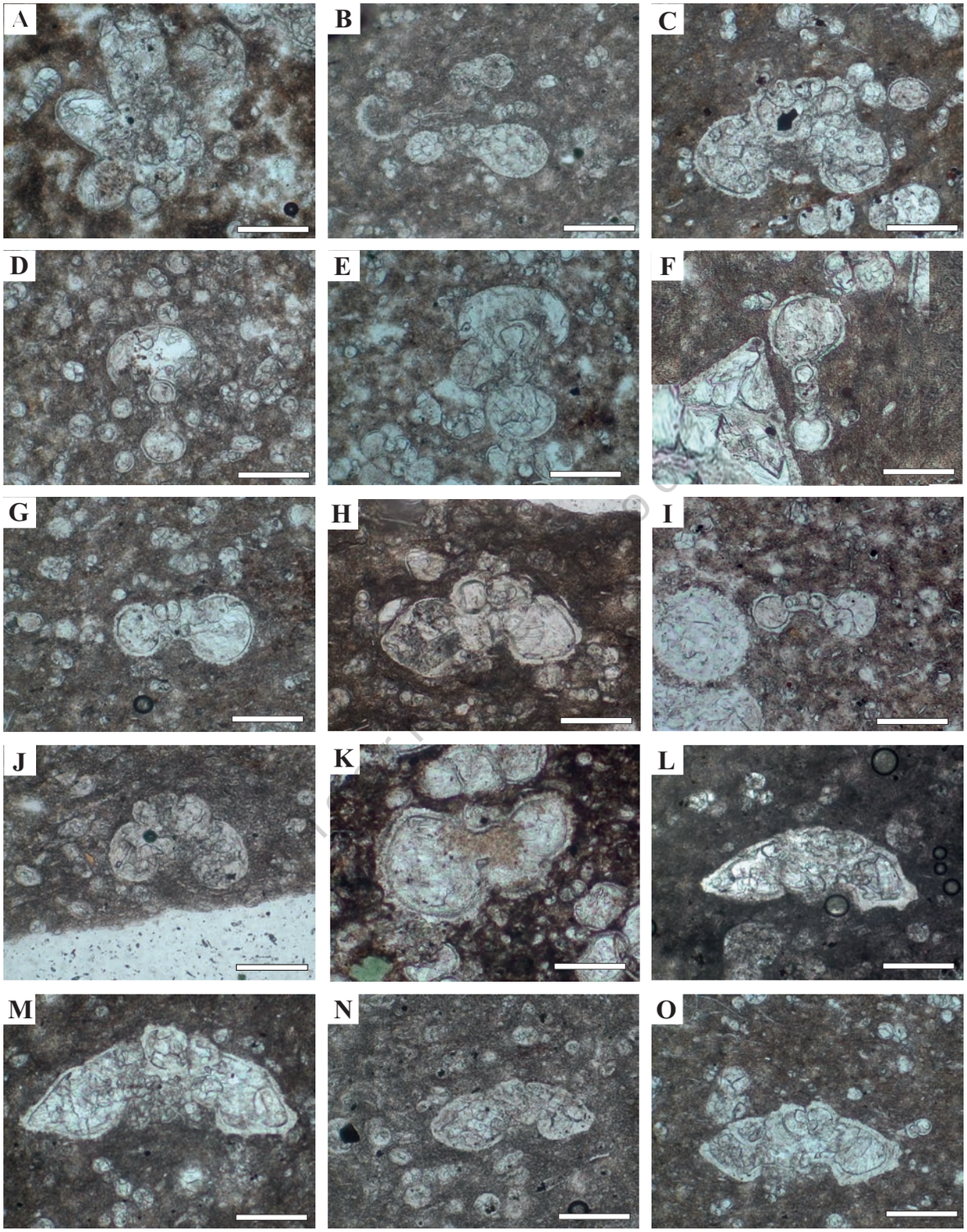
A
B
C
D
E
F
G
H
I
J
K
L
M
N
O

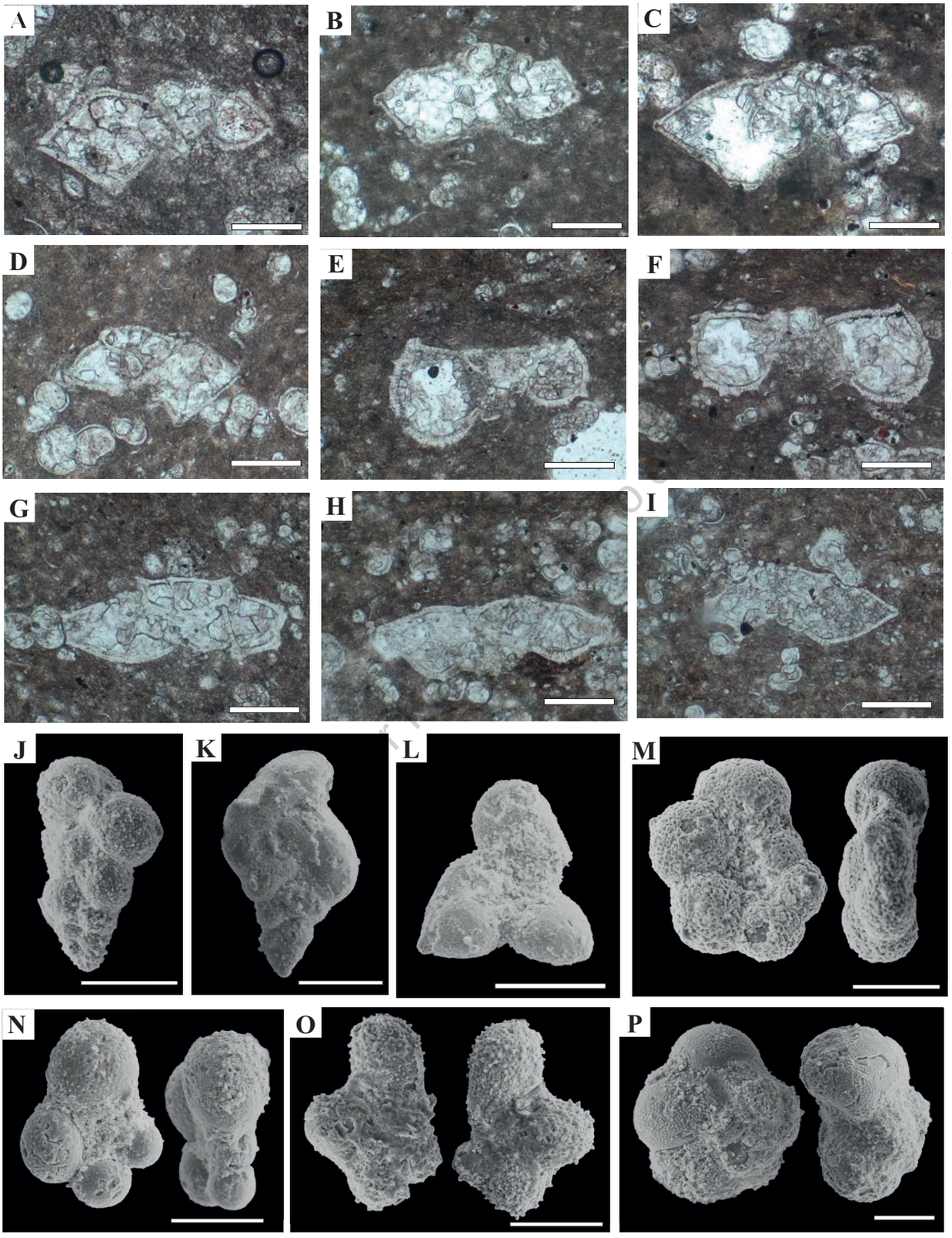
A
B
C
D
E
F
G
H
I
J
K
L
M
N
O
P

Fig. 6. A–B. *Rotalipora cushmani* (Morrow), samples 96, 117.5 and 119, C. *Rotalipora* sp., sample 117.5, **D.** *Thalmanninella greenhornensis* (Morrow), sample 117.5, **E–F.** *Helvetoglobotruncana helvetica* (Bolli), samples 132 and 134, **G**. *Dicarinella canaliculata* (Reuss), sample 146, **H**. *Dicarinella primitiva* (Dalbiez), sample 147, **I.** *Marginotruncana* sp., sample 140, **J.** *Planoheterohelix* cf. *reussi* (Cushman), sample 105, **K**. *Laeviheterohelix pulchra* (Brotzen), sample 134, **L.** *Schackoina cenomana* (Schako), sample 119, **M**. *Planohedbergella ultramicra* (Subbotina), sample 119, **N–O.** *Clavihedbergella simplex* (Morrow), samples 108.5 and 119.5, **P.** *Whiteinella* sp., sample 117. Scale bars equal 100 µm.

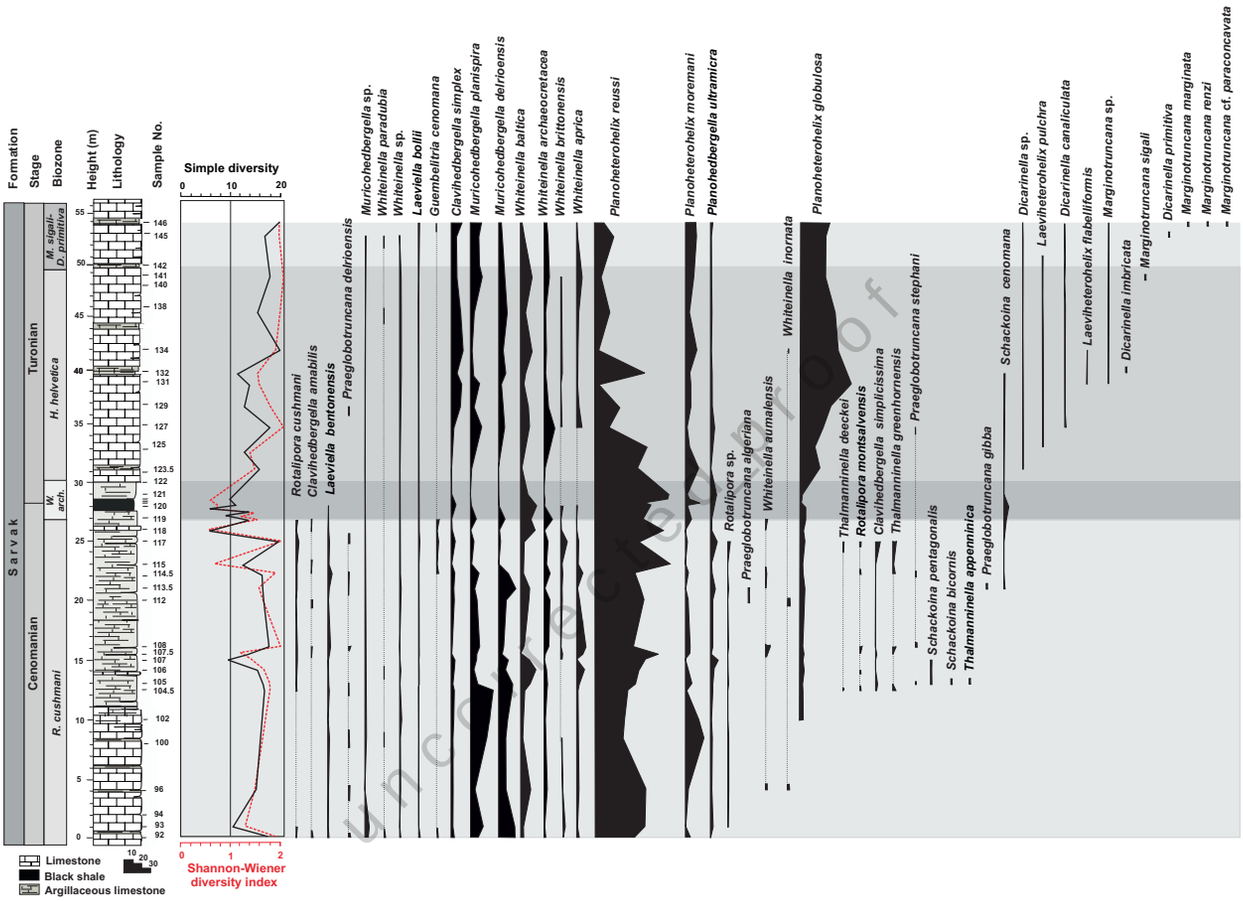

Fig. 7. Stratigraphic distribution and abundance of planktonic foraminifera species in the upper Cenomanian to upper Turonian succession of the Tang-e Bawlek section. Different grey bands are illustrated to differentiate the vertical range of each biozone.

conoidea, *Pithonella ovalis*, *P. sphaerica*, and *P. trejoi*, and), with *P. sphaerica* being notably more abundant than the others.

In the Tang-e Bawlek section, a relatively narrow interval (3 m thick) separates the HO of *R. cushmani* (27 m, Figs. 4 and 7) from the LO of *H. helvetica* (sample 122 at 30 m, Fig. 4), thereby delineating the *Whiteinella archaeocretacea* Zone with latest Cenomanian through early Turonian age (Premoli Silva & Verga 2004, Coccioni & Premoli Silva 2015). The association of this biozone is mainly represented by *Planoheterohelix, Whiteinella* (mostly *W. baltica*), *Muricohedbergella*, and *Clavihedbergella*.

The highly proliferation of biserial forms (*Planoheterohelix*) and radially elongated chambers (*C. simplex*) along with the HO of *L. bentonensis* at 28 m all occurred within this narrow zone (Fig. 7). The thickness of this biozone is notably reduced, significantly less than the 14 m reported by Navidtalab et al. (2019) in the Chenar-Bashi section, 10 km away from the

Tang-e Bawlek section, and 19 m-thick in the Lar Anticline (Kalanat & Vaziri-Moghaddam 2019). A comparable thickness of approximately 4.3 m thick for this biozone has been documented in the Fars Subzone (Bagherpour et al. 2023). In the studied interval, the LO of *W. archaeocretacea* preceding the LO of *P. algeriana*, which is much lower than what was proposed by Premoli Silva & Verga (2004) and Coccioni & Premoli Silva (2015). In the ZFTB the LO of this species was also recorded in the upper half of the *R. cushmani* Zone (Navidtalab et al. 2019, Kalanat & Vaziri-Moghaddam 2019).

The LO of *H. helvetica* at 30 m (sample 122, Fig. 4) marks the base of *H. helvetica* Zone, which is defined as the Total Range of the nominated taxon with late early Turonian through late middle Turonian age (Premoli Silva & Verga 2004, Coccioni & Premoli Silva 2015). This index species was solely documented through thin sections, representing an almost continuous occurrence from the base to the top of the zone (from 30 m to 50 m). The planktonic foraminiferal association of this zone is mainly represented by *Planoheterohelix*, *Muricohedbergella*, *Whiteinella*, *Clavihedbergella*, *Dicarinella*, and scattered specimens of *Marginotruncana*. *Dicarinella imbricata*, *D. canaliculata*, *D. hagni*, *Marginotruncana sigali*, and *M. schneegansi* first appear in this zone. The LO of *D. primitiva* was found in the sample 140 (at 48 m, Fig. 4), at the upper part of the *H. helvetica* Zone. This is slightly lower than previously documented at the base of the *Dicarinella primitiva-Marginotruncana sigali* Partial Range Zone (Premoli Silva & Verga 2004). Falzoni et al. (2016) also identified the specimens that exhibited similarities to the lateral view of the holotype of *D. primitiva* as *D.* cf. *primitiva*. This classification was due to uncertainties arising from the lack of clear morphological characteristics of *D. primitiva* specimens found within the middle of the *W. archaeocretacea* Zone

In the Vocontian Basin (SE France) and Eastbourne (SE England), the LO of the genus *Marginotruncana* was reported within the upper part of the *W. archaeocretacea* Zone and *R. cushmani* Zone, respectively (Falzoni et al. 2016, Falzoni & Petrizzo 2020). Consistent with our findings, the LO of the genus *Marginotruncana* was also recorded within the lower part of *H. helvetica* Zone in many localities (Coccioni & Premoli Silva 2015, Kalanat et al. 2016, Ezampanah et al. 2018, Navidtalab et al. 2019, Salhi et al. 2022).

The HO of *H. helvetica* in the sample 142 (50 m, Fig. 4) defines the base of the *Dicarinella primitiva-Marginotruncana sigali* Zone with latest middle Turonian to late Turonian age. The upper boundary of this zone was not sampled in the studied section. The planktonic foraminiferal assemblage in this zone is dominated by *Planoheterohelix*, primarily *P. globulosa*, along with fewer occurrences of whiteinellids, dicarinellids, and muricohedbergelids. The main characteristic of this zone is the gradual emergence of the double-keeled marginotruncanids (*Marginotruncana renzi*, *M. pseudolinneiana*, and *M. marginata*).

4.3. Planktonic foraminiferal assemblages

The hemipelagic facies of the Sarvak Formation in the Tang-e Bawlek notably hosts well-preserved planktonic foraminifera. The simple diversity and Shannon-Wiener diversity index of planktonic foraminifera, range between 6 to 20 and 0.6 to 2.29, respectively (Fig. 7). Planktonic foraminifera in this interval are represented by four morphotype groups including: biserial, non-keeled and keeled trochospiral, and planispiral-pseudoplanispiral (Fig. 8).

Throughout the studied section biserial morphotypes (mainly represented here by *Planoheterohelix*) are by far the most abundant groups and constitute a significant fraction of the planktonic foraminifera assemblage, typically averaging about 60% (Fig. 8). Their highest abundance occurs within the *W. archaeocretacea* Zone, where they dominate the planktonic foraminiferal assemblages with the values up to 97%. They are represented mainly by *Planoheterohelix* and to a lesser extent *Laeviheterohelix* (Fig. 7). After the biserial morphotypes, the non-keeled trochospiral morphotype (*Whiteinella*, *Muricohedbergella*, and *Clavihedbergella*) represent the second most frequently identified components (average 33%) (Figs. 7 and 8). The planispiral and pseudoplanispiral forms (*Laeviella*, *Planohedbergella* and *Schackoina*) with mean values of 3.4% are ranked as the third most common morphotype (Fig. 8). Finally, the last frequent morphotypes in the studied section are attributed to the keeled trochospiral morphotypes (*Thalmanninella*, *Rotalipora*, *Dicarinella*, *Helvetoglobotruncana*, *Marginotruncana*, and *Praeglobotruncana*) (average 1.6%).

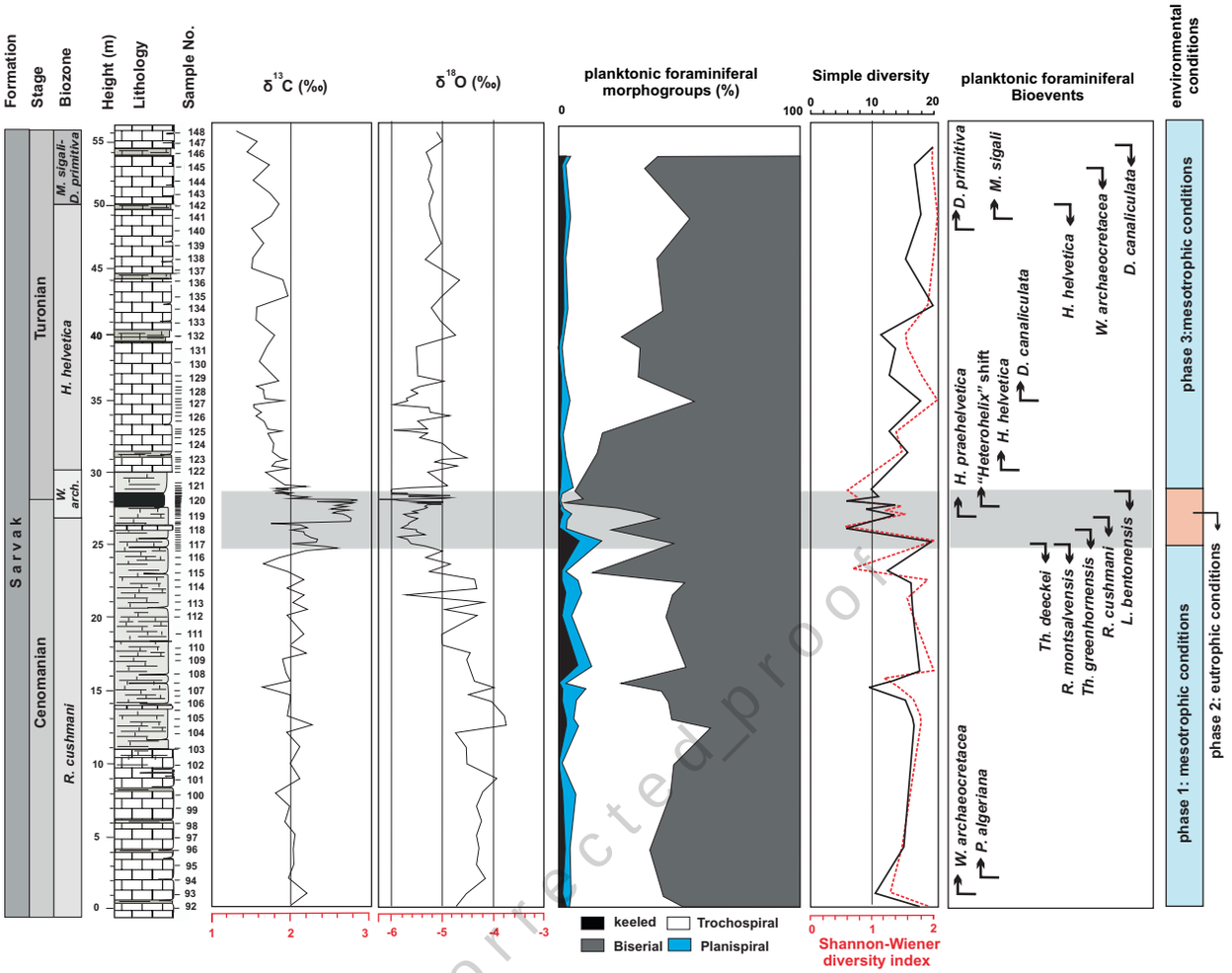

Fig. 8. Stratigraphic relationship between carbon and oxygen stable isotope data, identified morphotypes, simple diversity, main planktonic foraminiferal bio-events and paleoecological data in the studied section. The grey band is illustrated to signify and delineate the boundaries of the OAE2 interval, as well as its influence on paleoenvironmental conditions, which is referred to as phase 2 in the manuscript.

4.4. Carbon and oxygen stable isotope analysis and carbonate content variations

The isotope ratios measured on the bulk carbonates are shown in Figures 8 and 9 and listed in Supplementary Table S3. In addition, a blowup of the $\delta^{13}C$ profile in the interval straddling the CTB, is reported in figure 9 together with the carbonate content percentage.

The $\delta^{18}O$ values range from -6.23 to -3.77‰ (Fig. 8), being slightly depleted (~ 1–2‰) concerning good-to-exceptional preserved foraminifera tests from coeval, low palaeolatitude sites (O'Brien et al. 2017). Furthermore, high sample by sample variability of the ratios suggests a possible effect of diagenetic alteration on highly susceptible $\delta^{18}O$ marine bulk carbonate. Hence, an interpretation of the $\delta^{18}O$ values in terms of paleotemperatures was refused in this paper. In contrast, the δ13C values, between 1.34 to 2.86‰, fall within the range of the Cretaceous biotic calcite (e.g., Stoll & Schrag 2000, Sprovieri et al. 2013, Navidtalab et al. 2019), excluding possible effects of vital isotopic disequilibrium (McConnaughey 1989, Wefer & Berger 1991, Norris 1998). Moreover, the lack of a substantial correlation between δ13C and δ18O ($r = 0.17$, $P = 0.06$, $n = 123$) testifies the absence of overprinting produced by cement and micritic matrix that would record the isotopic composition of pore fluids during burial or meteoric diagenesis. The result of this process should be an offset towards more negative values of both

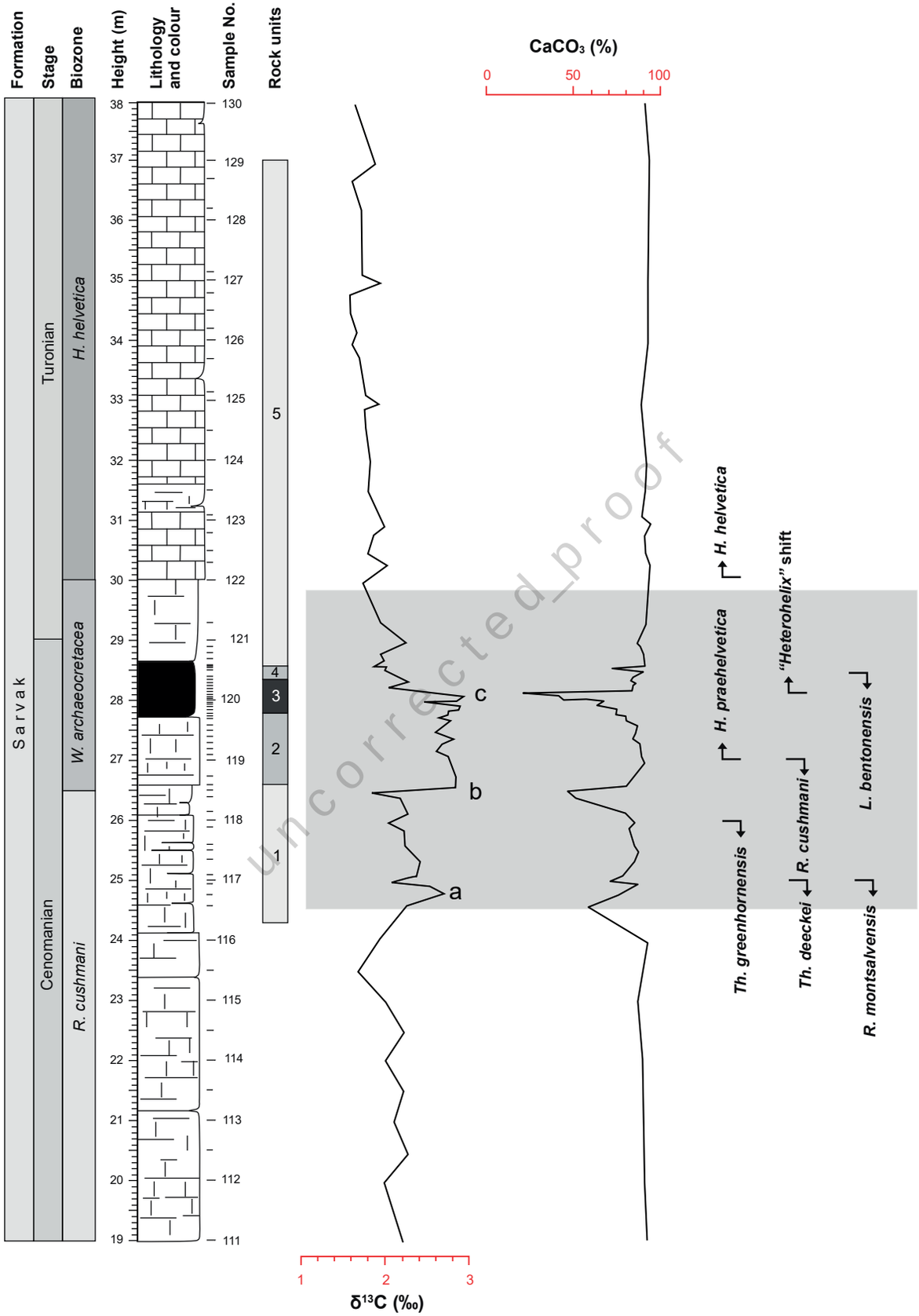
Formation
Stage
Biozone
Height (m)
Lithology and colour
Sample No.
Rock units
Sarvak
Turonian
Cenomanian
H. helvetica
W. archaeocretacea
R. cushmani
CaCO3 (%)
0
50
100
δ13C (‰)
1
2
3
a
b
c
H. helvetica
H. praehelvetica
"Heterohelix" shift
Th. greenhornensis
Th. deeckei
R. cushmani
L. bentonensis
R. montsalvensis
uncorrected_proof

Fig. 9. Relevant biozonations, lithological units, $\delta^{13}C$ records, carbonate content and, main planktic foraminifera bio-events across the CTBE in the Tang-e Bawlek section.

δ18O and δ13C and a strong correlation between them (Hajikazemi et al. 2010, Jeans et al. 2012, Montañez & Crossey 2018, Cramer & Jarvis 2020).

Accordingly, it can be assumed that the carbon isotope signature from the Tang-e Bawlek section is well preserved and can be used as a reference to describe the main CTBE trends and events in the Tethys realm.

Actually, the $\delta^{13}C$ depth profile shows a trend similar to the well documented in many CTB bulk $\delta^{13}C$ curves worldwide (see Discussion). In particular, in the lower 24 m of the section, the $\delta^{13}C$ curve indicates minimal variations (the values fall between 1.66 and 2.24‰). This part is characterized by a short positive peak ($\delta^{13}C$ = 2.24‰) in correspondence with a shale layer at 12.5 m and by two negative excursions at 15 and 23.5 m ($\delta^{13}C$ = 1.66‰ in both cases) (Fig. 8). The CTB interval is characterized by a well-marked positive $\delta^{13}C$ isotope excursion between 24 m and 28.5 m. The high-resolution sampling of this portion enabled us to discriminate within this excursion, the first peak at 24.78 m ($\delta^{13}C$ = 2.60‰) as well as a plateau in which the highest ratios of the whole section are recorded ($\delta^{13}C$ = 2.69‰ in average). The latter one extends from 26.60 to 28.15 m with the maximum $\delta^{13}C$ of 2.86‰ reached at 28.1 m. Finally, after a drop to 1.69‰ at 30 m, the uppermost part of the section is characterized by a progressive decrease in $\delta^{13}C$. The CaCO3 content, as depicted in the carbonate curve (Fig. 9), exhibits three distinct declines 57.25%, 45.60% and 19.54%, recorded at 24.6 m, 26.5 m and 28.15 m, respectively. They well align with the highest δ13C ratios, while the higher CaCO3 contents characterize limestones and argillaceous limestones throughout the investigated portion of the Sarvak Formation.

5. Discussion

5.1. Carbon stable isotope correlation

Before discussing the bio-events and delving into the palaeoecological and palaeoenvironmental aspects characterizing the Tang-e Bawlek section, and in consideration of the temporal interval spanned by the studied section, it is essential to evaluate the stratigraphic correlation with coeval sections in the world. It is well-established that the CTB interval is globally characterized by high burial rates of organic carbon (^{12}C) in the marine realm, leading to enrichment of the carbon isotope ratios both in marine carbonates and in organic carbon. The well-known positive excursion in the $\delta^{13}C$ is unanimously considered to be the geochemical signature of the OAE2 (Schlanger & Jenkyns 1976, Jenkyns 1980, Schlanger et al. 1987, Scholle & Arthur 1980, Tsikos et al. 2004).

Figure 10 shows the correlation of the $\delta^{13}C$ profile from this study with two high-resolution reference $\delta^{13}C$ curves: (i) the Global Boundary Stratotype of the Pueblo section (Rock Canyon Anticline, Colorado, US Western Interior Basin) chosen as the reference of the sub-excursions characterizing the CTBE (Caron et al. 2006), and (ii) the Eastbourne reference section (English Chalk, Southern England, Boreal Sea; Paul et al. 1999, Pearce et al. 2009, Jarvis et al. 2011). The Tang-e Bawlek section is also compared with two additional sections from the ZFTB: the Lar Anticline (Vaziri-Moghaddam & Kalanat 2020) and Cham-e-Zeytoon section (Bagherpour et al. 2023).

5.1.1. The Cenomanian/Turonian boundary Event (CTBE)

The CTBE is globally characterized by a distinctive positive $\delta^{13}C$ excursion that is further well-defined by three positive peaks known as a, b and c (Gale et al. 2005, Caron et al. 2006, Pearce et al. 2009, Jarvis et al. 2011). In the studied section, the three mentioned peaks are distinctly discernible in the carbon isotope record, as well as in the carbonate content curve (Figs. 9 and 10). In particular, the lower positive excursion (2.60‰), attributes to peak a, was recognized in the Tang-e Bawlek section at the top of *R. cushmani* Zone at 24.78 m (Figs. 8 and 9). After a distinct drop, the carbon isotope ratio raises up to the second shift at 26.60 and 26.75 m of 2.77 and 2.78‰, respectively, correlatable with the peak b falling right at the passage with the *W. archaeocretacea* Zone. The overlying plateau (1.5 meter), globally observed in the upper part of the OAE2 (Fig. 10), ends in the Tang-e Bawlek section at 28.1 m with the highest $\delta^{13}C$ value recorded (2.86‰) corresponding with peak c (Figs. 8 and 9). This peak,

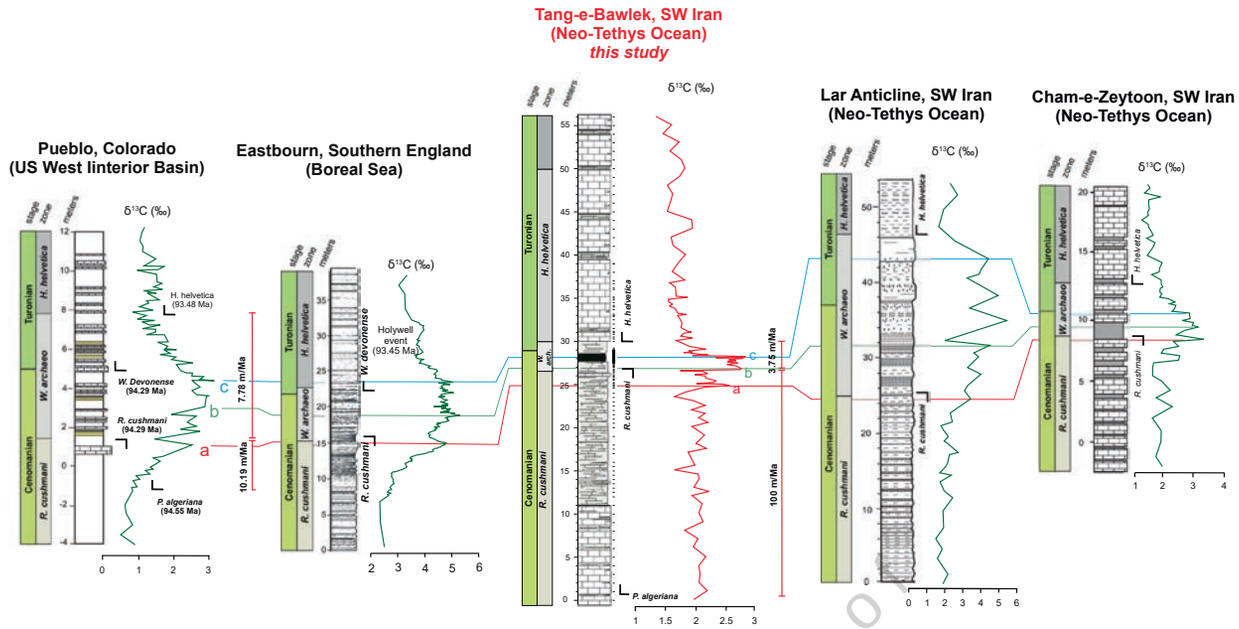

Fig. 10. Correlation of the carbonate $\delta^{13}C$ records between the studied Tang-e-Bawlek section with Pueblo section ($\delta^{13}C$ and bio-events data from Caron et al. 2006), Eastbourne section (data from Paul et al. 1999. Pearce et al. 2009 and Jarvis et al. 2011), Lar Anticline section (reinterpreted $\delta^{13}C$ data from Vaziri-Moghaddam & Kalanat 2020) and Cham-e-Zeytoon section (data from Bagherpour et al. 2023). The red, green and light blue lines mark the three CTB $\delta^{13}C$ peaks as defined in the Pueblo and Eastbourne reference sections. The ages of bio-events are from Falzoni et al. (2018). The sedimentation rate was calculated in Pueblo and Tang-e-Bawlek sections based on the age of zonal markers (LO of *P. algeriana*, HO of *R. cushmani*, and LO of *H. helvetica*) in the two intervals.

which is placed at the middle part of the *W. archaeocretacea* Zone is the most reliable criterion to proximate the CTB (Jarvis et al. 2006, 2011; Falzoni et al. 2018; Gale et al. 2019), in the lack of the ammonite *Watinoceras devonense* (Kennedy et al. 2000, 2005).

5.2. Bio-events in the Tang-e Bawlek section

Despite the wide distribution and extensively utilize of planktonic foraminiferal bio-events for correlation of pelagic and hemipelagic successions, the ecological preferences of each species act as limiting factors that may influence their stratigraphic distribution (Falzoni et al. 2018). Consequently, assuming global synchronicity of these bio-events is not warranted (Falzoni et al. 2018). To address this problem, researchers are increasingly using high-resolution carbon-isotope stratigraphy, which is synchronously registered across multiple sections, along with bio-events from different fossil groups (Pratt & Threlkeld 1984; Arthur et al. 1987; Tsikos et al. 2004; Jarvis et al. 2006, 2011; Jenkyns 2010; Falzoni et al. 2018). The response of biotic assemblages to the sudden ecological perturbation, such as what happened at the CTB, exhibits striking similarity across various sections located in both low and mid-latitudes (Falzoni et al. 2018, Falzoni & Petrizzo 2020). Therfore, some of those biota extinction/turnover levels linked to the OAE2 impacts appear synchronous and potentially used for supra-regional correlations (Tsikos et al. 2004, Caron et al. 2006, Elderbak et al. 2014, Falzoni et al. 2018, Bagherpour et al. 2023).

In the Tang-e Bawlek section, the HOs of *Th. deeckei* and *R. montsalvensis* were detected above peak a of the $\delta^{13}C$ profile (Figs. 7–9). With respect to peak a, the HO of *R. montsalvensis* was documented at various stratigraphic levels. In Eastbourne section (Falzoni et al. 2018) and Oued Ettalla section (Salhi et al. 2022), it was recorded slightly below peak a, while at the Gongzha section, it was recorded much lower than this peak (Bomou et al. 2013). At Bottaccione-Contessa composite section, this bio-event precedes the end of the *Th. greenhornensis* Subzone (Coccioni

& Premoli Silva 2015). According to Falzoni et al. (2018) and Falzoni & Petrizzo (2020) the HO of *Th. deeckei* consistently occurs below peak a on the $\delta^{13}C$ curve. The HO level of *Th. greenhornensis* is generally found to be identical with *Th. deeckei* in most localities, both of which were recorded below peak a (Falzoni et al. 2016; Gale et al. 2019; Keller et al. 2021; Falzoni & Petrizzo 2020, 2022). However, in some localities this bio-event is just aligned with peak a (Bagherpour et al. 2023) or slightly above it (Bidgood & Simmons 2023).

In the Tang-e Bawlek section, both HO levels of *Th. greenhornensis* and *R. cushmani* were documented above peaks a and b, respectively (Figs. 8 and 9). Falzoni & Petrizzo (2020 and references therein) recorded the HO of *R. cushmani* below peak a (Clot Chevalier section, France), between peaks a and b (Eastbourne section, England and Pont d'Issole section, France), at/slightly below peak b (Lar Anticline, Iran), above peak b (Ganuza section, Spain and Tarfaya section, Morocco).-

Typically, the extinction level of *L. bentonensis* was recognized above the HO of *R. cushmani* in the lower part of the *W. archaeocretacea* Zone (Elderbak et al. 2014, Coccioni & Premoli Silva 2015, Falzoni et al. 2016, Kalanat & Vaziri-Moghaddam 2019, Falzoni & Petrizzo 2020, Petrizzo et al. 2021, Salhi et al. 2022, Bidgood 6 Simmons 2023) and stands out as a consistently reliable and isochronous bio-event for the latest Cenomanian, particularly at low to mid-latitudes (Elderbak & Leckie 2016; Falzoni et al. 2016, 2018; Gale et al. 2019; Petrizzo et al. 2021). This bio-event was recorded between peaks a and b of $\delta^{13}C$ profile (Falzoni & Petrizzo 2020), somewhat aligned with the level of peak b (Falzoni et al. 2016, 2018) and above peak b (Tarfaya section, Morocco and Lar Anticline, Iran). In the current research, this bio-event was detected slightly below the highest $\delta^{13}C$ values (peak c). In summary, the stepwise extinctions of single-keeled foraminifera (*Th. deeckei*, *Th. greenhornensis*, and *R. cushmani*) at the top of the *R. cushmani* Zone, followed by HO of *La. bentonensis* at the lower part of *W. archaeocretacea* Zone, are approximately simultaneous across low to mid-latitudes and provide a reliable basis for regional correlation (Falzoni et al. 2018).

The "*Heterohelix*" shift (Leckie 1985) as a significant bio-event is documented at various stratigraphic levels, spanning from below $\delta^{13}C$ peak a to above $\delta^{13}C$ peak b (Keller et al. 2001, 2008; Coccioni & Luciani 2004). In the studied section, this bio-event aligns with the position of peak c.

It is noteworthy that the LO of *H. praehelvetica* was also documented just slightly above the peak b in the Tang-e Bawlek section. According to published researches, the LO of this bio-event varies from much lower than the HO of *R. cushmani* (Desmares et al. 2007, Bagherpour et al. 2023), slightly below peak a (Caron et al. 2006, Falzoni et al. 2018), to above peak c (Salhi et al. 2022). All of these findings support the unreliability of this bio-event for cross-latitude correlation (Petrizzo et al. 2021 and references therein).

The LO of the *H. helvetica*, which was detected in the studied section just 2 m above peak c, is frequently utilized to establish the lower part of the Turonian Stage in numerous low latitude sections. The LO of this index species was documented in various stratigraphic intervals between peaks b and c of $\delta^{13}C$ profile (Pearce et al. 2009), above peak c (Falzoni et al. 2018) or within the $\delta^{13}C$ values of Holywell and Lulworth events (Wendler 2013, Jarvis et al. 2015, Wendler et al. 2016). In Gubbio, this bio-event was observed approximately 2 meters above the "Bonarelli" black shale horizon after the $\delta^{13}C$ excursion of OAE2 (Wendler 2013 and references therein). Several factors make the LO of *H. helvetica* unreliable for defining the base of the Turonian Stage and for global correlations: 1) the rarity or sporadic occurrence of the taxon at the beginning of its stratigraphic range (Huber & Petrizzo 2014, Falzoni et al. 2016, 2018), 2) variations in taxonomic interpretations by different authors along with the transitional evolution from its ancestor, *H. praehelvetica* (Huber & Petrizzo 2014), 3) its absence in the higher latitudes and nearshore or marginal settings (Wendler 2013, Huber & Petrizzo 2014), and 4) due to the possible diachronous nature of this event at low latitudes (Grosheny et al. 2006, Desmares et al. 2007, Robaszynski et al. 2010, Huber & Petrizzo 2014, Falzoni et al. 2018).

The interval from 12 to 20 m (samples 104 to 112) is represented mainly by a packstone rich in filaments, planktonic foraminifera and calcispheres. Filaments are supposed to be small, thin bivalve larva shells or crinoidal plates (Mülayim et al. 2021), that thrived in the eutrophic conditions (Jefferies & Milton 1965, Caron et al. 2006). This event was recognized in the other parts of the Tethys Ocean within *W. archaeocretacea* Zone and utilized for tracking and correlating the CTB (Caron et al. 2006, Robaszynski et al. 2010, Bomou et al. 2013, Kalanat & Vaziri-Moghaddam 2019). In the Tang-e Bawlek section, this event was identified in the *P. algeriana* Subzone much lower than the CTB. Consequently, it cannot be considered as a reliable bio-

event for supra-regional correlation, and making its synchronicity questionable.

5.3. Planktonic foraminiferal assemblages and Palaeoenvironmental implications

Various biotic and abiotic factors could influence planktonic foraminifera's vertical and horizontal distribution in the water column (Petrizzo 2001). Within the Cretaceous, three primary communities of planktonic foraminifera have been identified: opportunistic (r-strategists), specialist (k-strategists) and r/k-mode intermediate foraminifera (Premoli Silva & Sliter 1999, Petrizzo 2002, Coccioni & Luciani 2005). The r-strategists comprise small-sized with simple morphology, thriving in unstable eutrophic conditions. The k-strategists are characterized by large-sized, primarily keeled complex morphotypes, adopted to oligotrophic environments (stable conditions). The r/k-mode intermediate foraminifera are considered to be adapted to the intermediate mesotrophic conditions. By integrating all the obtained data, three distinct phases, interpreted in terms of changes in paleoenvironmental conditions, can be identified in the Tang-e Bawlek section (Fig. 8).

5.3.1. Phase 1 (late Cenomanian; base of the section to 25 m)

This phase is characterized by a high sedimentation rate of 100 m/mys in the studied section (Figs. 8, 10 and Supplementary Table S2). Throughout this phase, high abundance and diversity of planktonic foraminifera occupying various ecological niches were recognized in both thin sections and washed samples. Biserial morphotypes dominates the planktonic foraminiferal assemblages of this phase. Small simple morphologies of r-strategists including muricohedbergellids (*M. planispira* and *M. delrioensis*), clavihedbergelids (*C. simplex*) and r-k intermediate strategists whiteinellids (*W. baltica*, *W. brittonensis* and *W. archaeocretacea*) are consistently present in nearly all samples, exhibiting varying abundances. The r and r-k strategists are considered to be indicators of eutrophic conditions in unstable paleoenvironments (Jarvis et al. 1988; Leckie et al. 1998, 2002; Keller & Pardo 2004; Omaña et al. 2014).

Single-keeled (rotaliporids and thalmanninelids) and double-keeled morphotypes (dicarinellids) were typically recorded in small quantities (Figs. 7 and 8). Actually the highest abundance of the keeled morphotype occurs in the *R. cushmani* Zone within this phase (Fig. 8). *Rotalipora* and *Thalmanninella* as oligotrophic fauna are believed to inhabit deep layers of the water column close to the thermocline depth (Leckie et al. 1998; Petrizzo 2002; Falzoni & Petrizzo 2020, 2022). A relatively thick and stratified upper water column has been suggested for these deep-dweller morphotypes to complete their life cycle (Petrizzo & Gale 2022 and references therein).

In addition to planktonic foraminifera, pithonellids are also abundant in this phase (Figs. 2, 3B–C and 4). As typical Tethyan thermophilic planktonic fossils, pithonellids exhibited a distribution restricted to 40° N and S of the equator, a pattern influenced by both latitudinal and facies-environmental factors (Kauffman & Johnson 1988, Dias-Brito 2000). Their bloom pointing to the conditions of well-mixed surface waters with normal-salinity and good oxygenation (Hart 1991; Dias-Brito 2000; Wendler et al. 2002a, b; Wilmsen 2003), typically occurring at times of maximum sea-level transgression and elevated temperatures (Dias-Brito 2000).

Within the studied section, a distinct relationship exists between this group of microfossils and lithology. In the lower portion of the section up to 22 m (sample 114), where carbonate facies prevail, pithonellids consistently dominate the microfossil assemblage (Figs. 2 and 3B). Upsection their abundance decreases sharply with the deposition of shaly layers. The remarkable association of pithonellid-rich microfacies with fine-grained carbonate accumulations in deep shelf to shallow bathyal environments implies that they thrived in carbonate-dominated ecosystems (Dias-Brito 2000, Flügel 2010; Omaña et al. 2014 and references therein).

The hypothesis is further strengthened by the absences of pithonellids in siliciclastic deposits and oceanic sediments (argillaceous marls and shales) (Dias-Brito 2000). Their association with r-strategists planktic foraminifera, suggests that they may be considered as opportunistic organisms well-adapted to eutrophic conditions (Coccioni & Luciani 2004, Omaña et al. 2014). Furthermore, their co-occurrence with keeled morphotypes (rotaliporids and thalmanninelids) indicates that these organisms could also thrived in deeper habitats. According to Dias-Brito (2000), pithonellids bloom in oligotrophic-mesotrophic conditions with other planktonic organisms with heavy tests. Wendler et al. (2002c) and Vink (2004) argued that palaeoenvironmental reconstructions using calcispheres require a

species level approach, since different species exhibit markedly variable environmental preferences. *Pithonella sphaerica*, as a species indicative of eutrophic conditions, represents the most opportunistic of the all pithonellids (Wendler et al. 2002a, b). The consistent dominance of this species is thought to reflect high carbonate production, elevated primary productivity and an enhanced nutrient supply (Jarvis et al. 1988, Noël et al. 1995, Gale et al. 2000, Wilmsen 2003, Pearce et al. 2009, Omaña et al. 2014). The prevalence of pithonellids coupled with the rarity of oligotrophic keeled morphotypes, suggesting a shift toward a higher trophic regime, specifically reflecting mesotrophic environmental conditions.

5.3.2. Phase 2 (CTB interval; 25 to 29 m)

Notable changes in planktonic foraminifera compositions occurred during this phase, resulted in a substantial decline in both their abundance and diversity. The key characteristics of this phase are: 1) a thin dark grey shale layer (unit 3 in Fig. 9), 2) a low sedimentation rate about 3.75 m/mys (Fig. 10) and consequent development of a condensed horizon rich in glauconite and phosphate, 3) a notable decrease in carbonate (CaCO3) content in compare to the three well-known peaks associated with OAE2 (Fig. 9), 4) the extinction of deep dwellers, k-strategists (i.e., rotaliporids and thalmanninellids) and rare occurrences of keeled morphotypes, 5) the predominance and proliferation of biserial taxa (i.e. *Planoheterohelix*), 6) a significant and worldwide correlatable positive excursion in $\delta^{13}C$, 7) a notable decrease in the proportion of calcispheres, and 8) low diversity of planktonic foraminifera (Figs. 4 and 8).

These characteristics reflect a shift in the paleoenvironmental conditions from more stable mesotrophic regime (phase 1) to highly stressed, eutrophic, and less stratified surface waters favoring opportunistic taxa (phase 2).

The development of eutrophic conditions in the surface waters prompted the expansion of the OMZ, thereby inhibiting the flourishing of large, deep-dwelling taxa (e.g., Leckie, 1985, Huber et al. 1999, Keller & Pardo, 2004, Falzoni et al. 2018, Salhi et al. 2022). Huber et al. (1999) proposed that warming of deep waters during the latest Cenomanian could have triggered a breakdown in water column stratification, impacting the life cycle of species inhabiting the deepest environments and, consequently, contributing to their extinction.

The extinction of *Laeviella bentonensis*, as an intermediate or thermocline dweller (Keller et al. 2001, Coccioni & Luciani 2005), suggests its greater sensitivity to environmental perturbations than other planispiral and non-keeled morphotypes (Leckie et al. 1998).

Notably, *Planoheterohelix* reaches its highest abundance (up to 97%) in both thin section and washed samples within the *W. archaeocretacea* Zone, coinciding with the OAE2 isotope excursion (Figs. 3C, 4, 7 and 8). The consistently high percentage of this opportunistic taxon throughout the dark grey shale interval signifies conditions of high stress and extreme oxygen deficiency (Leckie, 1985, Leckie et al. 1998, Huber et al. 1999, Keller et al. 2001, Coccioni & Luciani 2004, Caron et al. 2006, Bomou et al. 2013, Falzoni et al. 2018, Salhi et al. 2022). Other r-strategists and intermediate forms such as muricohedbergelids (*M. delrioensis* and *M. planispira*), whiteinellids (*W. baltica* and *W. archaeocretacea*), *Planohedbergella ultramicra* and a to a lesser extent *Schackoina cenomana* are minor constituents of this assemblage. The dominance of *P. reussi* (r-strategists) coupled with high abundances of other small surface dwellers points to elevated nutrient levels in near-surface waters (Petrizzo 2002, Coccioni & Luciani 2005).

5.3.3. Phase 3 (early to late Turonian; 29 to 55 m)

This phase initiates above the peak c of the $\delta^{13}C$ record, and seems to indicate a gradual restoration of the pre-OAE2 conditions (Fig. 8). Similar to the most other localities, the palaeoecological data suggest only a stepwise environmental recovery. The lower half of the *H. helvetica* Zone being still dominated by surface-dwellers opportunistic planktonic foraminiferal assemblages and rare indeterminate specimens of dicarinellids. Despite a marked decline in their overall abundance, biserial morphotypes still comprise a substantial proportion of the identified morphotypes above the CTB. The only conspicuous change within this group is the gradual increase in *P. globulosa* and a pronounced reduction in *P. reussi* (Fig. 7).

From 33 m (sample 125) upward, planktonic foraminifera exhibit a gradual increase in abundance and diversity. The abundance of *Dicarinella* species increases from the middle of the *H. helvetica* Zone and extends upward. The appearance of k-strategists complex morphotypes (marginotruncanids), mostly documented through thin sections, characterize the top of

the measured interval, corresponding to the *D. primitiva-M. sigali* Zone. *Laeviella* and *Planohedbergella* as planispiral morphotypes display a nearly continuous distribution. The high diversity and co-occurrence of various morphotypes within this part of the studied section reflect palaeoenvironmental changes and a shift towards more stable, oligotrophic conditions similar to those prevailed during phase 1. Perhaps owing to this environmental stability, new ecological niches were gradually occupied by newly evolved specialized taxa (Petrizzo 2002).

5.4. Sedimentological aspects of the CTB in the studied section

The hemipelagic facies of the Sarvak Formation is characterized by a muddy matrix rich in planktonic foraminifera and calcispheres suggesting deposition in a low energy, open marine environment below storm wave-base (Geel 2000, Ghabeishavi et al. 2009, Flügel 2010). From the lithological point of view, the CTB interval in the Tang-e Bawlek section is characterized by a dark grey shaly layer (about 1 m thick), followed by a thin hemipelagic argillaceous limestone layer rich in planktonic foraminifera and associated glauconite and phosphate minerals. This interval with a very low sedimentation rate (3.7 m/mys), is interpreted as a condensed horizon (Fig. 3E–F), indicative of sediment starvation in shelf and low energy deep-marine settings (Wilson 1975, Allouc 1990, Mutti & Bernoulli 2003, Flügel 2010, Föllmi et al. 2015, Christ et al. 2015, Richiano et al. 2019). Glauconite formation in shelf environments typically requires specific conditions including mixed redox environments near the OMZ, high productivity, low sedimentation rates, low-energy level, minimal terrigenous input, low turbulence, and an ample supply of iron and potassium (Odin & Matter 1981, Mozley & Carothers 1992, Malone et al. 2002, Nourmohamad et al. 2020).

A palaeodepth ranges between 50 and 550 m is regarded as an optimal setting for glauconization (Nourmohamad et al. 2020 and references therein). Glauconites within the specified horizon exhibit a green to dark green color and mostly lobate shape, suggest relatively high compositional maturity (Amorosi 1995, McCracken et al. 1996, Udgata 2007). Upwelling regime can trigger eutrophic conditions and high biological productivity in the surface waters subsequently enhancing organic matter supply to the sea floor and promoting phosphate precipitation in the vicinity of the OMZ (Glenn et al. 1988, Jarvis et al. 1994, Mutti & Bernoulli 2003, Föllmi et al. 2008; Brandano et al. 2016 and references therein). An alternative hypothesis "low-productivity phosphogenic model", highlights the importance of bacterial/microbial breakdown of organic matter below the sediment-seawater interface in enriching interstitial phosphate and releasing dissolved phosphate into the pore waters (Mutti & Bernoulli 2003 and references therein, Scopelliti et al. 2010, Banerjee et al. 2012; Christ et al. 2015). The presence of pyrite, a typical mineral found in organic-rich sediments, implies the activity of sulfate reducing bacteria and the development of anoxic environments (Shen et al. 2007, Nourmohamad et al. 2020).

The precipitation of the authigenic minerals (glauconite, phosphate, pyrite), is typical of sediments associated with condensed sections and basin starvation (Mitchum & Van Wagoner 1991, Föllmi 2016). The environmental conditions of the studied section during the CTB, as documented by hemipelagic limestones rich in glauconite and phosphate minerals, low sedimentation rate, and highly eutrophic conditions, well correspond to the development of a condensed horizon in a deep low oxygenated environment.

Therefore, it is possible to assume that the tectonic activity in the ZFTB, which caused sediment exposure and unconformities in the Fars and Dezful subzones, may have had a limited effect on this part of the basin. Actually, deep marine conditions prevailed in the Lurestan Subzone as the depocenter or focal point of the sedimentary basin. This is in accord with Wynd (1965) and Moeini et al. (2023) interpretations that considered the Lurestan Subzone, as the distal portion of an evolving platform, extended along the passive margin of the northeastern part of the Arabian Plate, from the Early to middle Cretaceous.

6. Conclusions

Utilizing a multidisciplinary approach integrating field observations, facies analysis, biostratigraphy, and carbon isotopic data demonstrate that, unlike most of the ZFTB where CTB is marked by a regional unconformity due to sea-level fall, this part of the basin lacks evidences of subaerial exposure or significant changes in the microfacies types (e.g., from pelagic to benthic). Instead, this boundary is here solely characterized by deep marine grey to dark grey argillaceous limestones and black shales, rich in planktonic foraminifera and associated with glauconite and phosphate grains and a low sedimentation rate. The hemiplegic interval of the Sarvak Formation in the Tang-e

Bawlek section was possibly deposited in an intra-shelf basin in the Lurestan Subzone.

LOs and HOs of important zonal markers have enabled the identification of four planktonic foraminifera biozones across the studied section, which suggest a late Cenomanian-late Turonian age. In stratigraphic order, the main identified bio-events in this interval, include the LO of *P. algeriana*, HOs of *Th. deeckei*, *Th. greenhornensis*, *R. cushmani* and *La. bentonensis* followed by the LO and HO of *H. helvetica* and finally appearance of dicarinellids and marginotruncanids. The correlation of the newly conducted high-resolution $\delta^{13}C$ record with other reference sections has allowed comprehensive documentation of the CTBE in the Tang-e Bawlek section. Recognition of the three distinctive peaks that globally characterize the CTB carbon isotope excursion, gives the studied section the potential to serve as a key reference section for global correlations. The paleoecological reconstruction of the studied interval highlighted three major changes in the depositional environment: 1) Pre-OAE2 interval with a high sedimentation rate and largely meso-eutrophic regime, 2) OAE2 interval with highly eutrophic conditions suitable for high proliferation of opportunistic taxa (especially *Planoheterohelix*) during the development of OMZ. This phase is represented by a dark grey shale layer followed by a low sedimentation rate that resulted in the formation of a condensed horizon, and 3) Post-OAE2 interval which indicates a gradual recovery of paleoenvironmental conditions and appearance of new genera and species.

Acknowledgements. The authors are grateful to Ali Solymani for his help during the field trips. Financial support for isotope analysis was provided by FFR 2022/2023 G. Scopelliti. Part of the study was funded by grants to Y. Ezampanah and H. Mohseni via Vice-President Research Affair of Bu-Ali Sina University. Critical review and constructive comments of the editor and anonymous reviewers improved the quality of the manuscript.

References

Alavi, M. (2004). Regional stratigraphy of the Zagros fold-thrust belt of Iran and its proforeland evolution. *American Journal of Science, 304*(1), 1–20. https://doi.org/10.2475/ajs.304.1.1

Alavi, M. (2007). Structures of the Zagros fold-thrust belt in Iran. *American Journal of Science, 307*(9), 1064–1095. https://doi.org/10.2475/09.2007.02

Allouc, J. (1990). Quaternary crusts on slopes of the Mediterranean Sea: A tentative explanation for their genesis. *Marine Geology, 94*(3), 205–238. https://doi.org/10.1016/0025-3227(90)90070-Z

Amorosi, A. (1995). Glaucony and sequence stratigraphy: A conceptual framework of distribution in siliciclastic sequences. *Journal of Sedimentary Research, B65*, 419–425.

Ando, A., & Huber, B. T. (2007). Taxonomic revision of the Late Cenomanian planktonic foraminifera *Rotalipora Greenhornensis. Journal of Foraminiferal Research, 37*(2), 160–174. https://doi.org/10.2113/gsjfr.37.2.160

Arthur, M. A., Schlanger, S. O., & Jenkyns, H. C. (1987). The Cenomanian-Turonian oceanic anoxic event, II. Palaeoceanographic controls on organic-matter production and preservation. In J. Brooks & A. J. Fleet (Eds.), Geological Society, London, Special Publications: *Vol. 26. Marine Petroleum Source Rocks* (pp. 401–420). https://doi.org/10.1144/GSL.SP.1987.026.01.25

Asadi Mehmandosti, E., Asadi, A., Daneshian, J., Adam, D., Woods, A. D., & Loyd, S. J. (2021). Evidence of Mid-Cretaceous carbon cycle perturbations and OAE2 recorded in Cenomanian to middle Campanian carbonates of the Zagros fold–thrust belt basin, Iran. *Journal of Asian Earth Sciences, 218*, 104863. https://doi.org/10.1016/j.jseaes.2021.104863

Bagherpour, B., Mehrabi, H., Faghih, A., Vaziri-Moghaddam, H., & Omidvar, M. (2021). Tectono-eustatic controls on depositional setting and spatial facies distribution of Coniacian-Santonian sequences of the Zagros Basin in Fars area, S. Iran. *Marine and Petroleum Geology, 129*, 105072. https://doi.org/10.1016/j.marpetgeo.2021.105072

Bagherpour, B., Nkemata, A. F., Vaziri-Moghaddam, H., Blattmann, T. M., & Mohtadi, M. (2023). Paleoenvironmental significance of the carbon isotope record across the Cenomanian-Turonian transition and the Oceanic Anoxic Event 2 (OAE2) in the southeastern Neotethys, Zagros, Iran. *Cretaceous Research, 150*, 105574. https://doi.org/10.1016/j.cretres.2023.105574

Banerjee, S., Chattoraj, S. L., Saraswati, P. K., Dasgupta, S., & Sarkar, U. (2012). Substrate control on formation and maturation of glauconites in the Middle Eocene Harudi Formation, western Kutch, India. *Marine and Petroleum Geology, 30*(1), 144–160. https://doi.org/10.1016/j.marpetgeo.2011.10.008

Barclay, R. S., McElwain, J. C., & Sageman, B. B. (2010). Carbon sequestration activated by a volcanic CO2 pulse during Ocean Anoxic Event 2. *Nature Geoscience, 3*(3), 205–208. https://doi.org/10.1038/ngeo757

Barrier, E., & Vrielynck, B. (2008). Map 6: Cenomanian (99.6–93.5 Ma). In E. Barrier & B. Vrielynck (Eds.), Palaeotectonic Maps of the Middle East-Tectono-Sedimentary-Palinspastic Maps from the Late Norian to Pliocene. Commission for the Geological Map of the World. Paris: CGMW/CCGM.

Bidgood, M. D., & Simmons, M. D. (2023). Cenomanian planktonic foraminifera, bioevents and biozonation – A brief review. *Newsletters on Stratigraphy, 56*(2), 125–156. https://doi.org/10.1127/nos/2022/0717

Bomou, B., Adatte, T., Tantawy, A. A., Mort, H., Fleitmann, D., Huang, Y., & Föllmi, K. B. (2013). The expression of the Cenomanian–Turonian oceanic anoxic event in Tibet. *Palaeogeography, Palaeoclimatology, Palaeoecology, 369*, 466–481. https://doi.org/10.1016/j.palaeo.2012.11.011

Brandano, M., Westphal, H., Mateu-Vicens, G., Preto, N., & Obrador, A. (2016). Ancient upwelling record in a phosphate hardground (Tortonian of Menorca, Balearic Islands, Spain). *Marine and Petroleum Geology, 78*, 593–605. https://doi.org/10.1016/j.marpetgeo.2016.07.017

Bromhead, A. D., van Buchem, F. S. P., Simmons, M. D., & Davies, R. B. (2022). Sequence stratigraphy, palaeogeography and petroleum plays of the Cenomanian–Turonian succession of the Arabian Plate: An updated synthesis. *Journal of Petroleum Geology, 45*(2), 119–161. https://doi.org/10.1111/jpg.12810

Caron, M., Robaszynski, F., Amedro, F., Baudin, F., Deconinck, J. F., Hochuli, P., . . . Tribovillard, N. (1999). Estimation de la durée de l'événement anoxique global au passage Cénomanien/Turonien. Approche cyclostratigraphique dans la formation Bahloul en Tunisie centrale. *Bulletin de la Société Géologique de France*, *170*, 145–160.

Caron, M., Dall'Agnolo, S., Accarie, H., Barrera, E., Kauffman, E. G., Amédro, F., & Robaszynski, F. (2006). High–resolution stratigraphy of the Cenomanian–Turonian boundary interval at Pueblo (USA) and Wadi Bahloul (Tunisia): Stable isotope and bio–events correlation. *Géobios, 39*(2), 171–200. https://doi.org/10.1016/j.geobios.2004.11.004

Caron, M., & Premoli Silva, I. (2007). New description of the rotaliporid species Brotzeni and Globotruncanoides sigal, 1948 based on re-examination of type material. *Rivista Italiana di Paleontologia e Stratigrafia*, *113*, 525–530.

Christ, N., Immenhauser, A., Wood, R. A., Darwich, Kh., & Niedermayr, A. (2015). Petrography and environmental controls on the formation of Phanerozoic marine carbonate hardgrounds. *Earth-Science Reviews, 151*, 176–226. https://doi.org/10.1016/j.earscirev.2015.10.002

Coccioni, R., & Luciani, V. (2004). Planktonic foraminifera and environmental changes across the Bonarelli Event (OAE2, latest Cenomanian) in its type area: A high–resolution study from the Tethyan reference Bottaccione section (Gubbio, Central Italy). *Journal of Foraminiferal Research, 34*(2), 109–129. https://doi.org/10.2113/0340109

Coccioni, R., & Luciani, V. (2005). Planktonic foraminifers across the Bonarelli Event (OAE2, latest Cenomanian): The Italian record. *Palaeogeography, Palaeoclimatology, Palaeoecology, 224*(1-3), 167–185. https://doi.org/10.1016/j.palaeo.2005.03.039

Coccioni, R., & Premoli Silva, I. (2015). Revised Upper Albian–Maastrichtian planktonic foraminiferal biostratigraphy and magneto–stratigraphy of the classical Tethyan Gubbio section (Italy). *Newsletters on Stratigraphy, 48*(1), 47–90. https://doi.org/10.1127/nos/2015/0055

Cramer, B. D., & Jarvis, I. (2020). Carbon Isotope Stratigraphy. In *Geologic Time Scale* (pp. 309–343). Elsevier.

Desmares, D., Grosheny, D., Beaudoin, B., Gardin, S., & Gauthier-Lafaye, F. (2007). High-resolution stratigraphic record constrained by volcanic ash beds at the Cenomanian-Turonian boundary in the Western Interior Basin, USA. *Cretaceous Research, 28*(4), 561–582. https://doi.org/10.1016/j.cretres.2006.08.009

Dias-Brito, D. (2000). Global stratigraphy, palaeobiogeography and palaeoecology of Albian–Maastrichtian pithonellid calcispheres: Impact on Tethys configuration. *Cretaceous Research, 21*(2-3), 315–349. https://doi.org/10.1006/cres.2000.0196

Elderbak, K., Leckie, R. M., & Tibert, N. E. (2014). Paleoenvironmental and paleoceanographic changes across the Cenomanian-Turonian Boundary Event (Oceanic Anoxic Event 2) as indicated by foraminiferal assemblages from the eastern margin of the Cretaceous Western Interior Sea. *Palaeogeography, Palaeoclimatology, Palaeoecology, 413*, 29–48. https://doi.org/10.1016/j.palaeo.2014.07.002

Elderbak, K., & Leckie, R. M. (2016). Paleocirculation and foraminiferal assemblages of the Cenomanian-Turonian Bridge Creek Limestone bedding couplets: Productivity vs. dilution during OAE2. *Cretaceous Research, 60*, 52–77. https://doi.org/10.1016/j.cretres.2015.11.009

Ernst, R. E., & Youbi, N. (2017). How Large Igneous Provinces affect global climate, sometimes cause mass extinctions, and represent natural markers in the geologic record. *Palaeogeography, Palaeoclimatology, Palaeoecology, 478*, 30–52. https://doi.org/10.1016/j.palaeo.2017.03.014

Esfandyari, M., Mohseni, H., & Heidari, M. (2023). Facies analysis, depositional sequences and platform evolution of the Sarvak Formation (late Albian-Turonian) in the Zagros Basin, West of Iran. *Journal of African Earth Sciences, 198*, 104811. https://doi.org/10.1016/j.jafrearsci.2022.104811

Ezampanah, Y., Sadeghi, A., Jamali, A., & Adabi, M. (2013). Biostratigraphy of the Garau Formation (Berriasian?–lower Cenomanian) in central part of Lurestan zone, northwest of Zagros, Iran. *Cretaceous Research, 46*, 101–113. https://doi.org/10.1016/j.cretres.2013.06.007

Ezampanah, Y., Sadeghi, A., Scopelliti, G., Adabi, M. H., & Jamali, A. M. (2018). Planktonic foraminifera biozones and isotope stratigraphy of the Cenomanian-Turonian boundary in the western part of the Kopet-Dagh Basin, NE Iran. *Journal of African Earth Sciences, 147*, 657–670. https://doi.org/10.1016/j.jafrearsci.2018.07.011

Ezampanah, Y., Di Lucia, M., Yazdi-Moghadam, M., & Zaghbib-Turki, D. (2022). Planktonic foraminiferal distribution of the Late Cretaceous to late Paleocene deposits of the Bandar Abbas area (Zagros Belt, SW Iran): An update of the bio-and lithostratigraphic framework. *Journal of African Earth Sciences, 185*, 104392. https://doi.org/10.1016/j.jafrearsci.2021.104392

Falzoni, F., Petrizzo, M. R., Jenkyns, H. C., Gale, A. S., & Tsikos, H. (2016). Planktonic foraminiferal biostratigraphy and assemblage composition across the Cenoma-

nian-Turonian boundary interval at Clot Chevalier (Vocontian Basin, SE France). *Cretaceous Research*, *59*, 69–97. https://doi.org/10.1016/j.cretres.2015.10.028

Falzoni, F., Petrizzo, M. R., Caron, M., Leckie, R. M., & Elderbak, K. (2018). Age and synchronicity of planktonic foraminiferal bioevents across the Cenomanian–Turonian boundary interval (Late Cretaceous). *Newsletters on Stratigraphy*, *51*(3), 343–380. https://doi.org/10.1127/nos/2018/0416

Falzoni, F., & Petrizzo, M. R. (2020). Patterns of planktonic foraminiferal extinctions and eclipses during Oceanic Anoxic Event 2 at Eastbourne (SE England) and other mid-low latitude locations. *Cretaceous Research*, *116*, 104593. https://doi.org/10.1016/j.cretres.2020.104593

Falzoni, F., & Petrizzo, M. R. (2022). Evidence for changes in sea-surface circulation patterns and ~20° equatorward expansion of the Boreal bioprovince during a cold snap of Oceanic Anoxic Event 2 (Late Cretaceous). *Global and Planetary Change*, *208*, 103678. https://doi.org/10.1016/j.gloplacha.2021.103678

Farzipour-Saein, A., Yassaghi, A., Sherkati, S., & Koyi, H. (2009). Basin evolution of the Lurestan region in the Zagros fold-and-thrust belt, Iran. *Journal of Petroleum Geology*, *32*(1), 5–19. https://doi.org/10.1111/j.1747-5457.2009.00432.x

Fletcher, B. J., Brentnall, S. J., Anderson, C. W., Berner, R. A., & Beerling, D. J. (2008). Atmospheric carbon dioxide linked with Mesozoic and early Cenozoic climate change. *Nature Geoscience*, *1*(1), 43–48. https://doi.org/10.1038/ngeo.2007.29

Flügel, E. (2010). *Microfacies of carbonate rocks, analysis interpretation and application* (2nd ed., pp. 1–976). Berlin: Springer-Verlag. https://doi.org/10.1007/978-3-642-03796-2

Föllmi, K. B., Gertsch, B., Renevey, J. P., de Kaenel, E., & Stille, P. (2008). Stratigraphy and sedi- mentology of phosphate-rich sediments in Malta and southeastern Sicily (latest Oligocene to early Late Miocene). *Sedimentology*, *55*(4), 1029–1051. https://doi.org/10.1111/j.1365-3091.2007.00935.x

Föllmi, K. B., Hofmann, H., Chiaradia, M., de Kaenel, E., Frijia, G., & Parente, M. (2015). Miocene phosphate-rich sediment in Salento (southern Italy). *Sedimentary Geology*, *327*, 55–71. https://doi.org/10.1016/j.sedgeo.2015.07.009

Föllmi, K. B. (2016). Sedimentary condensation. *Earth-Science Reviews*, *152*, 143–180. https://doi.org/10.1016/j.earscirev.2015.11.016

Gale, A. S., Smith, A. B., Monks, N. E. A., Young, J. A., Howard, A., Wray, D. S., & Huggett, J. M. (2000). Marine biodiversity through the Late Cenomanian–Early Turonian: Palaeoceanographic controls and sequence stratigraphic biases. *Journal of the Geological Society*, *157*(4), 745–757. https://doi.org/10.1144/jgs.157.4.745

Gale, A. S., Kennedy, W. J., Voigt, S., & Walaszczyk, I. (2005). Stratigraphy of the Upper Cenomanian–Lower Turonian Chalk succession at Eastbourne, Sussex, UK: Ammonites, inoceramid bivalves and stable carbon isotopes. *Cretaceous Research*, *26*(3), 460–487. https://doi.org/10.1016/j.cretres.2005.01.006

Gale, A. S., Jenkyns, H. C., Tsikos, H., van Breugel, Y., Sinninghe Damste, J. S., Bottini, C., . . . Wray, D. S. (2019). High-resolution bio-and chemostratigraphy of an expanded record of Oceanic Anoxic Event 2 (Late Cenomanian–Early Turonian) at Clot Chevalier, near Barrême, SE France (Vocontian Basin). *Newsletters on Stratigraphy*, *52*(1), 97–129. https://doi.org/10.1127/nos/2018/0445

Gangl, S. K., Moy, C. M., Stirling, C. H., Jenkyns, H. C., Crampton, J. S., Clarkson, M. O., . . . Porcelli, D. (2019). High-resolution records of Oceanic Anoxic Event 2: Insights into the timing, duration and extent of environmental perturbations from the palaeo-South Pacific Ocean. *Earth and Planetary Science Letters*, *518*, 172–182. https://doi.org/10.1016/j.epsl.2019.04.028

Geel, T. (2000). Recognition of stratigraphic sequences in carbonate platform and slope deposits: Empirical models based on microfacies analysis of Palaeogene deposits in southeastern Spain. *Palaeogeography, Palaeoclimatology, Palaeoecology*, *155*(3-4), 211–238. https://doi.org/10.1016/S0031-0182(99)00117-0

Ghabeishavi, A., Vaziri-Moghaddam, H., & Taheri, A. (2009). Facies distribution and sequence stratigraphy of the Coniacian–Santonian succession of the Bangestan Palaeohigh in the Bangestan Anticline, SW Iran. *Facies*, *55*(2), 243–257. https://doi.org/10.1007/s10347-008-0171-3

Ghabeishavi, A., Vaziri-Moghaddam, H., Taheri, A., & Taati, F. (2010). Microfacies and depositional environment of the Cenomanian of the Bangestan anticline, SW Iran. *Journal of Asian Earth Sciences*, *37*(3), 275–285. https://doi.org/10.1016/j.jseaes.2009.08.014

Ghasemi-Nejad, E., Hobbi, M. H., & Schiøler, P. (2006). Dinoflagellate and foraminiferal biostratigraphy of the Gurpi Formation (upper Santonian–upper Maastrichtian), Zagros Mountains, Iran. *Cretaceous Research*, *27*(6), 828–835. https://doi.org/10.1016/j.cretres.2006.03.013

Glenn, C. R., Arthur, M. A., Yeh, H. W., & Burnett, W. C. (1988). Carbon isotopic composition and lattice-bound carbonate of Peru–Chile margin phosphorites. *Marine Geology*, *80*(3-4), 287–307. https://doi.org/10.1016/0025-3227(88)90094-1

Glennie, K. W. (2000). Cretaceous tectonic evolution of Arabia's eastern plate margin: A tale of two oceans. *SEPM Special Publications*, *69*, 9–20. https://doi.org/10.2110/pec.00.69.0009

González-Donoso, J. M., Linares, D., & Robaszynski, F. (2007). The rotaliporids, a polyphyletic group of Albian-Cenomanian planktonic foraminifera: Emendation of genera. *Journal of Foraminiferal Research*, *37*(2), 175–186. https://doi.org/10.2113/gsjfr.37.2.175

Grosheny, D., Beaudoin, B., Morel, L., & Desmares, D. (2006). High-resolution biostratigraphy and chemostratigraphy of the Cenomanian–Turonian Boundary Event in the Vocontian Basin, S-E France. *Cretaceous*

Research, *27*(5), 629–640. https://doi.org/10.1016/j.cretres.2006.03.005

Hajikazemi, E., Al-Aasm, I. S., & Coniglio, M. (2010). Subaerial exposure and meteoric diagenesis of the Cenomanian–Turonian upper Sarvak Formation, southwestern Iran. *Special Publication – Geological Society of London*, *330*(1), 253–272. https://doi.org/10.1144/SP330.12

Hajikazemi, E., Al-Aasm, I. S., & Coniglio, M. (2012). Chemostratigraphy of Cenomanian–Turonian carbonates of the Sarvak Formation, Southern Iran. *Journal of Petroleum Geology*, *35*(2), 187–205. https://doi.org/10.1111/j.1747-5457.2012.00525.x

Hart, M. B. (1991). The Late Cenomanian calcisphere global bioevent. *Proceedings of the Ussher Society*, *7*, 413–417.

Haynes, S. J., Huber, B. T., & Macleod, K. G. (2015). Evolution and phylogeny of mid-Cretaceous (Albian–Coniacian) biserial planktic foraminifera. *Journal of Foraminiferal Research*, *45*(1), 42–81. https://doi.org/10.2113/gsjfr.45.1.42

Hollis, C. (2011). Diagenetic controls on reservoir properties of carbonate successions within the Albian–Turonian of the Arabian Plate. *Petroleum Geoscience*, *17*(3), 223–241. https://doi.org/10.1144/1354-079310-032

Hollis, C., & Sharp, I. (2011). Albian-Cenomanian-Turonian carbonate-siliciclastic systems of the Arabian Plate: Advances in diagenesis, structure and reservoir modelling: introduction. *Petroleum Geoscience*, *17*(3), 207–209. https://doi.org/10.1144/1354-079310-060

Huber, B. T., Leckie, R. M., Norris, R. D., Bralower, T. J., & CoBabe, E. (1999). Foraminiferal assemblage and stable isotopic change across the Cenomanian–Turonian boundary in the subtropical North Atlantic. *Journal of Foraminiferal Research*, *29*, 392–417.

Huber, B. T., & Petrizzo, M. R. (2014). Evolution and taxonomic study of the Cretaceous planktic foraminiferal genus *Helvetoglobotruncana* Reiss, 1957. *Journal of Foraminiferal Research*, *44*(1), 40–57. https://doi.org/10.2113/gsjfr.44.1.40

Huber, B. T., Petrizzo, M. R., Young, J. R., Falzoni, F., Gilardoni, S. E., Bown, P. R., & Wade, B. S. (2016). Pforams@microtax: A new online taxonomic database for planktonic foraminifera. *Micropaleontology*, *62*(6), 429–438. https://doi.org/10.47894/mpal.62.6.02

Huber, B. T., Petrizzo, M. R., & Falzoni, F. (2022). Taxonomy and phylogeny of Albian–Maastrichtian planispiral planktonic foraminifera traditionally assigned to *Globigerinelloides*. *Micropaleontology*, *68*(2), 117–183. https://doi.org/10.47894/mpal.68.2.01

Ištuk, Ž., Kampić, Š., Felja, I., Pavlović, M., Tudor, T., Jazvac, I., . . . Ćosović, V. (2023). Retrieving planktonic foraminifera from lithified rocks, examples from the Eocene limestones and marls (External Dinarides, Croatia). *MethodsX*, *10*, 102233. https://doi.org/10.1016/j.mex.2023.102233

James, G. A., & Wynd, J. G. (1965). Stratigraphic Nomenclature of Iranian Oil Consortium Agreement Area. *The American Association of Petroleum Geologists Bulletin*, *49*, 2182–2245.

Jarvis, I., Carson, G. A., Cooper, M. K. E., Hart, M. B., Leary, P. N., Tocher, B. A., . . . Rosenfeld, A. (1988). Microfossil assemblages and the Cenomanian–Turonian (Late Cretaceous) oceanic anoxic event. *Cretaceous Research*, *9*(1), 3–103. https://doi.org/10.1016/0195-6671(88)90003-1

Jarvis, I., Burnett, W. C., Nathan, Y., Almbaydin, F. S. M., Attia, A. K. M., Castro, L. N., . . . Zanin, Y. N. (1994). Phosphorite geochemistry: state of the art and environmental concerns. In K. B. Fo¨llmi (Ed.), *Concepts and Controversies in Phosphogenesis. Eclogae Geologicae Helveticae*, *87*, *643–700*.

Jarvis, I., Gale, A. S., Jenkyns, H. C., & Pearce, M. A. (2006). Secular variation in Late Cretaceous carbon isotopes: A new $\delta^{13}C$ reference curve for the Cenomanian–Campanian (99.6–70.6Ma). *Geological Magazine*, *143*(5), 561–608. https://doi.org/10.1017/S0016756806002421

Jarvis, I., Lignum, J. S., Gröcke, D. R., Jenkyns, H. C., & Pearce, M. A. (2011). Black shale deposition, atmospheric CO2 drawdown, and cooling during the Cenomanian–Turonian Oceanic Anoxic Event. *Paleoceanography*, *26*(3), PA3201. https://doi.org/10.1029/2010PA002081

Jarvis, I., Trabucho-Alexandre, J., Gröcke, D. R., Uličný, D., & Laurin, J. (2015). Intercontinental correlation of organic carbon and carbonate stable isotope records: Evidence of climate and sea-level change during the Turonian (Cretaceous). *The Depositional Record: a Journal of Biological, Physical and Geochemical Sedimentary Processes*, *1*(2), 53–90. https://doi.org/10.1002/dep2.6

Jeans, C., Hu, X., & Mortimore, R. (2012). Calcite cements and the stratigraphical significance of the marine δ13C carbonate reference curve for the Upper Cretaceous Chalk of England. *Acta Geologica Polonica*, *62*(2), 173–196. https://doi.org/10.2478/v10263-012-0008-9

Jefferies, R., & Milton, P. (1965). The mode of life of two Jurassic species of “Posidonia” (Bivalvia). *Palaeontology*, *8*, 156–185.

Jenkyns, H. C. (1980). Cretaceous anoxic events: From continents to oceans. *Journal of the Geological Society*, *137*(2), 171–188. https://doi.org/10.1144/gsjgs.137.2.0171

Jenkyns, H. C. (2010). Geochemistry of oceanic anoxic events. *Geochemistry, Geophysics, Geosystems*, *11*(3), Q03004. https://doi.org/10.1029/2009GC002788

Kalanat, B., Vahidinia, M., Vaziri-Moghaddam, H., & Mahmudy-Gharaie, M. H. (2016). Planktonic foraminiferal turnover across the Cenomanian-Turonian boundary (OAE2) in northeast of Tethys realm, Kopet-Dagh basin. *Geologica Carpathica*, *67*(5), 451–462. https://doi.org/10.1515/geoca-2016-0028

Kalanat, B., & Vaziri-Moghaddam, H. (2019). The Cenomanian/Turonian boundary interval deep-sea deposits in the Zagros Basin (SW Iran): Bioevents, carbon isotope record and palaeoceanographic model. *Palaeogeography, Palaeoclimatology, Palaeoecology*, *533*, 109238. https://doi.org/10.1016/j.palaeo.2019.109238

Kauffman, E. G., & Johnson, C. C. (1988). The morphological and ecological evolution of middle and Upper Cretaceous reef building rudistids. *Palaios, 3*(2), 194–216. https://doi.org/10.2307/3514530

Kariminia, S. M. (2004). Extraction of calcified Radiolaria and other calcified micro-fossils from micritic limestone utilizing acetic acid. *Micropaleontology, 50*(3), 301–306. https://doi.org/10.2113/50.3.301

Keller, G., Han, Q., Adatte, T., & Burns, S. (2001). Paleoenvironment of the Cenomanian–Turonian transition at Eastbourne England. *Cretaceous Research, 22*(4), 391–422. https://doi.org/10.1006/cres.2001.0264

Keller, G., & Pardo, A. (2004). Age and paleoenvironment of the Cenomanian–Turonian global stratotype section and point at Pueblo, Colorado. *Marine Micropaleontology, 51*(1-2), 95–128. https://doi.org/10.1016/j.marmicro.2003.08.004

Keller, G., Adatte, T., Berner, Z., Chellai, E. H., & Stueben, D. (2008). Oceanic events and biotic effects of the Cenomanian-Turonian Anoxic Event, Tarfaya Basin, Morocco. *Cretaceous Research, 29*(5-6), 976–994. https://doi.org/10.1016/j.cretres.2008.05.020

Keller, G., Nagori, M. L., Chaudhary, M., Reddy, A. N., Jaiprakash, B. C., Spangenberg, J. E., . . . Adatte, T. (2021). Cenomanian-Turonian sea-level transgression and OAE2 deposition in the Western Narmada Basin, India. *Gondwana Research, 94*, 73–86. https://doi.org/10.1016/j.gr.2021.02.013

Kennedy, W. J., Walaszczyk, I., & Cobban, W. A. (2000). Pueblo, Colorado, USA, Candidate Global Boundary Stratotype Section and Point for the base of the Turonian Stage of the Cretaceous and for the Middle Turonian substage, with a revision of the Inoceramidae (Bivalvia). *Acta Geologica Polonica, 50*, 295–334.

Kennedy, W. J., Walaszczyk, I., & Cobban, W. A. (2005). The Global Boundary Stratotype Section and Point for the base of the Turonian Stage of the Cretaceous: Pueblo, Colorado, USA. *Episodes, 28*(2), 93–104. https://doi.org/10.18814/epiiugs/2005/v28i2/003

Kuhnt, W., Herbin, J. P., Thurow, J., & Wiedmann, J. (1990). Distribution of Cenomanian–Turonian organic-facies in the western Mediterranean and along the adjacent Atlantic margin. In A. Y. Huc (Ed.), *Deposition of Organic Facies. American Association of Petroleum Geologists Studies in Geology, 30, 133–160*. https://doi.org/10.1306/St30517C10

Kuypers, M. M. M., Pancost, R. D., Nijenhuis, I. A., & Sinninghe Damsté, J. S. (2002). Enhanced productivity led to increased organic carbon burial in the euxinic North Atlantic basin during the late Cenomanian oceanic anoxic event. *Paleoceanography, 17*(4), 3–13. https://doi.org/10.1029/2000PA000569

Larson, R. L. (1991). Geological consequences of superplumes. *Geology, 19*(10), 963–966. https://doi.org/10.1130/0091-7613(1991)0192.3.CO;2

Leckie, R. M. (1985). Foraminifera of the Cenomanian–Turonian boundary interval, Greenhorn Formation, Rock Canyon Anticline, Pueblo, Colorado. In L. M. Pratt, E. G. Kauffman, & F. B. Zelt (Eds.), *Fine Grained deposits and Biofacies of the Cretaceous Western Interior Seaway: Evidence of Cyclic Sedimentary Processes. Society of Economic Paleontologists and Mineralogists. Field Trip Guidebook*, 139–149 pp.

Leckie, R. M., Yuretrich, R. F., West, O. L. O., Finkelstein, D., & Schmidt, M. (1998). Paleoceanography of the southwestern Western Interior Sea during the time of the Cenomanian–Turonian boundary (Late cCretaceous). In W. Dean & M. A. Arthur (Eds.), *Stratigraphy and paleoenvironments of the Cretaceous Western Interior Seaway. SEPM concepts in Sedimentology and Paleontology, 6, 101–126*.

Leckie, R. M., Bralower, T. J., & Cashman, R. (2002). Oceanic anoxic events and plankton evolution: Biotic response to tectonic forcing during the mid–Cretaceous. *Paleoceanography, 17*(3), 1041. https://doi.org/10.1029/2001PA000623

Leturmy, P., & Robin, C. (2010). Tectonic and stratigraphic evolution of Zagros and Makran during the Mesozoic–Cenozoic. *Special Publication – Geological Society of London, 330*(1), 1–4. https://doi.org/10.1144/SP330.1

Li, Y. X., Montañez, I. P., Liu, Z., & Ma, L. (2017). Astronomical constraints on global carbon-cycle perturbation during Oceanic Anoxic Event 2 (OAE2). *Earth and Planetary Science Letters, 462*, 35–46. https://doi.org/10.1016/j.epsl.2017.01.007

Malik, M. H., Chan, S. A., Babalola, L. O., & Kaminski, M. A. (2022). Optimization of the acetic acid method for microfossil extraction from lithified carbonate rocks: Examples from the Jurassic and Miocene limestones of Saudi Arabia. *MethodsX, 9*, 101828. https://doi.org/10.1016/j.mex.2022.101828

Malone, M. J., Claypool, G., Martin, J. B., & Dickens, G. R. (2002). Variable methane fluxes in shallow marine systems over geologic time: The composition of pore waters and authigenic carbonates on the New Jersey shelf. *Marine Geology, 189*(3-4), 175–196. https://doi.org/10.1016/S0025-3227(02)00474-7

McConnaughey, T. (1989). ^{13}C and ^{18}O isotopic disequilibrium in biological carbonates: I. Patterns. *Geochimica et Cosmochimica Acta, 53*(1), 151–162. https://doi.org/10.1016/0016-7037(89)90282-2

McCracken, S. R., Compton, J., & Hicks, K. (1996). Sequence stratigraphic significance of glaucony-rich lithofacies at site 903. In G. S. Mountain, K. G. Miller, P. Blum, C. W. Poagand, & D. C. Twichell (Eds.). *Proceedings of the Ocean Drilling Program, Scientific Results, College Station, Texas, 150*, 171–187.

Mehrabi, H., Navidtalab, A., Enayati, A. H., & Bagherpour, B. (2022). Age, duration, and geochemical signatures of paleo-exposure events in Cenomanian–Santonian sequences (Sarvak and Ilam formations) in SW Iran: Insights from carbon and strontium isotopes chemostratigraphy. *Sedimentary Geology, 434*, 106136. https://doi.org/10.1016/j.sedgeo.2022.106136

Mitchum, R. M., Jr., & Van Wagoner, J. C. (1991). High frequency sequences and their stacking patterns: Sequence-stratigraphic evidence of high-frequency eus-

tatic cycles. *Sedimentary Geology, 70*(2-4), 131–160. https://doi.org/10.1016/0037-0738(91)90139-5

Moeini, M., Rahimpour-Bonab, H., & Tavakoli, V. (2023). Evidence for Isolated Platform Development in the Cenomanian on the Passive Margin of Neotethys, Southwest Iran. *Minerals (Basel), 13*(6), 757. https://doi.org/10.3390/min13060757

Mohseni, H., & Zeybaram Javanmard, R. (2020). New data on sequence stratigraphy of the Sarvak Formation in Malekshahi city, (Ilam province) Zagros basin, Iran. *Marine and Petroleum Geology, 112*, 104035. https://doi.org/10.1016/j.marpetgeo.2019.104035

Montañez, I. P., & Crossey, L. J. (2018). Diagenesis. In W. M. White (Ed.), *Encyclopedia of Geochemistry* (pp. 353–362). Springer International Publishing. https://doi.org/10.1007/978-3-319-39312-4_35

Motiei, H. (2003). *Treatise on the geology of Iran: Stratigraphy of Zagros* (p. 497). Tehran: Geological Survey of Iran. (in Persian)

Mülayim, O., Yilmaz, I. O., Sari, B., & Ferré, B. (2021). 'Filament' marker beds in the Karababa-A Member (Turonian) of the Arabian platform, SE Turkey: Palaeo-environmental significance, stratigraphy and correlation potential. *Proceedings of the Geologists' Association, 132*, 188–198.

Mozley, P. S., & Carothers, W. W. (1992). Elemental and isotopic compositions of siderite in the Kuparuk Formation, Alaska: Effect of microbial activity and water/sediment interaction on early pore water chemistry. *Journal of Sedimentary Petrology, 62*, 681–692.

Murray, J. W. (1991). Ecology and distribution of benthic foraminifera. In J. J. Lee & O. R. Anderson (Eds.), *Biology of Foraminifera* (pp. 221–254). Academic Press.

Mutti, M., & Bernoulli, D. (2003). Early marine lithification and hardground development on a Miocene ramp (Maiella, Italy): Key surfaces to track changes in trophic resources in nontropical carbonate settings. *Journal of Sedimentary Research, 73*(2), 296–308. https://doi.org/10.1306/083102730296

Navidtalab, A., Rahimpour-Bonab, H., Huck, S., & Heimhofer, U. (2016). Elemental geochemistry and strontium-isotope stratigraphy of Cenomanian to Santonian neritic carbonates in the Zagros Basin, Iran. *Sedimentary Geology, 346*, 35–48. https://doi.org/10.1016/j.sedgeo.2016.10.003

Navidtalab, A., Heimhofer, U., Huck, S., Omidvar, M., Rahimpour-Bonab, H., Aharipour, R., & Shakeri, A. (2019). Biochemostratigraphy of an upper Albian–Turonian succession from the southeastern Neo-Tethys margin, SW Iran. *Palaeogeography, Palaeoclimatology, Palaeoecology, 533*, 109255. https://doi.org/10.1016/j.palaeo.2019.109255

Noël, D., Busson, G., Mangin, A. M., & Cornée, A. (1995). La distribution des Pithonelles dans le Campanien inférieur et moyen du Boulonnais (Nord de la France). Liasion avec les alternances craies/craies marneuses et implications environnementales et historiques. *Revue de Micropaléontologie, 38*, 245–255.

Nourmohamadi, M. S., Abdula, R. A., Albeyati, F., Sharezwri, A. O., Perot, E. M., Jassim, Sh. E., & Othman, N. H. (2020). Green glauconitic marl bed as a sequence stratigraphical key for interpretation of contact between Qamchuqa and Bekhme formations in Bekhal area, Kurdistan region, NE Iraq. *Buletin Persatuan Geologi Malaysia, 70*(1), 29–38. https://doi.org/10.7186/bg702020003

Norris, R. D. (1998). Recognition and Macroevolutionary significance of photosymbiosis in molluscs, corals, and foraminifera. In R. D. Norris & R. M. Corfield (Eds.), *Isotope Paleobiology and Paleoecology* (pp. 68–100). Pittsburgh: The Paleontological Society. https://doi.org/10.1017/S1089332600000401

O'Brien, C. L., Robinson, S. A., Pancost, R. D., Damste, J. S. S., Schouten, S., Lunt, D. J., . . . Farnsworth, A. (2017). Cretaceous sea-surface temperature evolution: Constraints from TEX86 and planktonic foraminiferal oxygen isotopes. *Earth-Science Reviews, 172*, 224–247. https://doi.org/10.1016/j.earscirev.2017.07.012

Odin, G. S., & Matter, A. (1981). De glauconiarum origine. *Sedimentology, 28*(5), 611–641. https://doi.org/10.1111/j.1365-3091.1981.tb01925.x

Omaña, L., Torres, J. R., López-Doncel, R., Alencáster, G., & López-Caballero, I. (2014). A pithonellid bloom in the Cenomanian-Turonian boundary interval from Cerritos in the western Valles–San Luis Potosí platform, Mexico: Paleoenvironmental significance. *Revista Mexicana de Ciencias Geológicas, 31*, 28–44.

Pancost, R. D., Crawford, N., Magness, S., Turner, A., Jenkyns, H. C., & Maxwell, J. R. (2004). Further evidence for the development of photic-zone euxinic conditions during Mesozoic oceanic anoxic events. *Journal of the Geological Society, 161*(3), 353–364. https://doi.org/10.1144/0016764903-059

Paul, C. R. C., Lamolda, M. A., Mitchell, S. F., Vaziri, M. R., Gorostidi, A., & Marshall, J. D. (1999). The Cenomanian–Turonian boundary at Eastbourne (Sussex, UK): A proposed European reference section. *Palaeogeography, Palaeoclimatology, Palaeoecology, 150*(1-2), 83–121. https://doi.org/10.1016/S0031-0182(99)00009-7

Pearce, M. A., Jarvis, I., & Tocher, B. A. (2009). The Cenomanian–Turonian boundary event, OAE2 and palaeoenvironmental change in epicontinental seas: New insights from the dinocyst and geochemical records. *Palaeogeography, Palaeoclimatology, Palaeoecology, 280*(1-2), 207–234. https://doi.org/10.1016/j.palaeo.2009.06.012

Petrizzo, M. R. (2001). Late Cretaceous planktonic foraminifera from Kerguelen Plateau (ODP Leg 183): New data to improve the Southern Ocean biozonation. *Cretaceous Research, 22*(6), 829–855. https://doi.org/10.1006/cres.2001.0290

Petrizzo, M. R. (2002). Palaeoceanographic and palaeoclimatic inferences from Late Cretaceous planktonic foraminiferal assemblages from the Exmouth Plateau (ODP Sites 762 and 763, eastern Indian Ocean). *Marine Micropaleontology, 45*(2), 117–150. https://doi.org/10.1016/S0377-8398(02)00020-8

Petrizzo, M. R., & Huber, B. T. (2006). Biostratigraphy and taxonomy of late Albian planktonic foraminifera from ODP Leg 171B (western North Atlantic Ocean). *Journal of Foraminiferal Research, 36*(2), 166–190. https://doi.org/10.2113/36.2.166

Petrizzo, M. R., Falzoni, F., & Premoli Silva, I. (2011). Identification of the base of the lower-to-middle Campanian Globotruncana ventricosa Zone: Comments on reliability and global correlations. *Cretaceous Research, 32*(3), 387–405. https://doi.org/10.1016/j.cretres.2011.01.010

Petrizzo, M. R., Caron, M., & Premoli Silva, I. (2015). Remarks on the identification of the Albian/Cenomanian boundary and taxonomic clarification of the planktonic foraminifera index species *globotruncanoides, brotzeni* and *tehamaensis*. *Geological Magazine, 152*(3), 521–536. https://doi.org/10.1017/S0016756814000478

Petrizzo, M. R., & Gilardoni, S. E. (2020). Planktonic foraminiferal biostratigraphy of late Albian-Cenomanian pelagic sequences from the Umbria-Marche basin (central Italy) and the Mazagan Plateau (northeast Atlantic Ocean). *Rivista Italiana di Paleontologia e Stratigrafia, 126*, 865–904.

Petrizzo, M. R., Watkins, D. K., MacLeod, K. G., Hasegawa, T., Huber, B. T., Batenburg, S. J., & Kato, T. (2021). Exploring the paleoceanographic changes registered by planktonic foraminifera across the Cenomanian-Turonian boundary interval and Oceanic Anoxic Event 2 at southern high latitudes in the Mentelle Basin (SE Indian Ocean). *Global and Planetary Change, 206*, 103595. https://doi.org/10.1016/j.gloplacha.2021.103595

Petrizzo, M. R., & Gale, A. S. (2022). Planktonic foraminifera document palaeoceanographic changes across the middle Cenomanian carbon-isotope excursion MCE 1: New evidence from the UK chalk. *Geological Magazine, 160*(2), 372–392. https://doi.org/10.1017/S0016756822000991

Piryaei, A. R., Reijmer, J. J. G., van Buchem, F. S. P., Yazdi-Moghadam, M., Sadouni, J., & Danelian, T. (2010). The influence of Late Cretaceous tectonic processes on sedimentation patterns along the northeastern Arabian plate margin (Fars Province, SW Iran). *Special Publication – Geological Society of London, 330*(1), 211–251. https://doi.org/10.1144/SP330.11

Piryaei, A. R., Reijmer, J. J. G., Borgomano, J., & van Buchem, F. S. P. (2011). Late Cretaceous Tectonic and sedimentary evolution of the Bandar Abbas area, Fars region, southern Iran. *Journal of Petroleum Geology, 34*(2), 157–180. https://doi.org/10.1111/j.1747-5457.2011.00499.x

Pratt, L. M., & Threlkeld, C. N. (1984). Stratigraphic Significance of $^{13}C/^{12}C$ Ratios in Mid-Cretaceous Rocks of the Western Interior. *Memoir – Canadian Society of Petroleum Geologists, 9*, 305–312.

Premoli Silva, I., & Sliter, W. V. (1999). Cretaceous paleoceanography: evidence from planktonic foraminiferal evolution. In E. Barrera & C. C. Johnson (Eds.), Geological Society of America Special Paper: *Vol. 332. the evolution of Cretaceous ocean-climatic system* (pp. 301–328). https://doi.org/10.1130/0-8137-2332-9.301

Premoli Silva, I., & Verga, D. (2004). P*ractical Manual of Cretaceous Planktonic Foraminifera*. In Verga and Rettori (Eds.), *International School on Planktonic Foraminifera, 3° Course: Cretaceous*. Universities of Perugia and Milan Tipografia Pontefelcino, Perugia (Italy).

Rahimpour-Bonab, H., Mehrabi, H., Enayati-Bidgoli, A. H., & Omidvar, M. (2012). Coupled imprints of tropical climate and recurring emersions on reservoir evolution of a mid-Cretaceous carbonate ramp, Zagros Basin, SW Iran. *Cretaceous Research, 37*, 15–34. https://doi.org/10.1016/j.cretres.2012.02.012

Rahimpour-Bonab, H., Mehrabi, H., Navidtalab, A., Omidvar, M., Enayati-Bidgoli, A. H., Sonei, R., . . . Izadi-Mazidi, E. (2013). Paleoexposure surfaces in Cenomanian-Santonian carbonate reservoirs in the Dezful Embayment, SW Iran. *Journal of Petroleum Geology, 36*(4), 335–362. https://doi.org/10.1111/jpg.12560

Razin, P., Taati, F., & van Buchem, F. S. P. (2010). Sequence stratigraphy of Cenomanian-Turonian carbonate platform margins (Sarvak Formation) in the high Zagros, SW Iran: An outcrop reference model for the Arabian plate. *Special Publication – Geological Society of London, 329*(1), 187–218. https://doi.org/10.1144/SP329.9

Razmjooei, M. J., Thibault, N., Kani, A., Dinarès-Turell, J., Pucéat, E., Shahriari, S., . . . Cocquerez, T. (2018). Integrated bio- and carbon-isotope stratigraphy of the Upper Cretaceous Gurpi Formation (Iran): A new reference for the eastern Tethys and its implications for large-scale correlation of stage boundaries. *Cretaceous Research, 91*, 312–340. https://doi.org/10.1016/j.cretres.2018.07.002

Richiano, S., Schwarz, E., Veiga, G. D., & Trentini, G. A. (2019). Non-depositional and erosional "offshore" bioeroded hardgrounds from the Lower Cretaceous of the Neuquén Basin, Argentina: Insights into their sequence-stratigraphic implications and controls. *Marine and Petroleum Geology, 104*, 1–10. https://doi.org/10.1016/j.marpetgeo.2019.03.020

Robaszynski, F., Zagrarni, M. F., Caron, M., & Amédro, F. (2010). The global bio-events at the Cenomanian-Turonian transition in the reduced Bahloul Formation of Bou Ghanem (central Tunisia). *Cretaceous Research, 31*(1), 1–15. https://doi.org/10.1016/j.cretres.2009.07.002

Sageman, B. B., Meyers, S. R., & Arthur, M. A. (2006). Orbital time scale and new C-isotope record for Cenomanian–Turonian boundary stratotype. *Geology, 34*(2), 125–128. https://doi.org/10.1130/G22074.1

Salhi, I., Elamri, Z., Bazeen, Y. S., Ahmad, F., Mahmoudi, S., & Farouk, S. (2022). Planktonic foraminifera and stable isotopes of the upper Cenomanian-middle Turonian in central Tunisia: Implications for bioevents synchronicity and paleoenvironmental turnover. *Cretaceous Research, 138*, 105291. https://doi.org/10.1016/j.cretres.2022.105291

Sarfi, M., Ghasemi-Nejad, E., Mahanipour, A., Yazdi-Moghadam, M., & Sharifi, M. (2015). Integrated biostratigraphy and geochemistry of the lower Cretaceous

Radiolarian Flood Zone of the base of the Garau Formation, northwest of Zagros Mountains, Iran. *Arabian Journal of Geosciences*, *8*(9), 7245–7255. https://doi.org/10.1007/s12517-014-1712-4

Schlanger, S. O., & Jenkyns, H. C. (1976). Cretaceous oceanic anoxic events: Causes and consequences. *Geologie en Mijnbouw*, *55*, 179–184.

Schlanger, S. O., Arthur, M. A., Jenkyns, H. C., & Scholle, P. A. (1987). The Cenomanian–Turonian Oceanic Anoxic Event, I. Stratigraphy and distribution of organic carbon-rich beds and the marine $\delta^{13}C$ excursion (pp. 371–399). London: Geological Society.

Scholle, P. A., & Arthur, M. A. (1980). Carbon isotope fluctuations in Cretaceous pelagic limestones; potential stratigraphic and petroleum exploration tool. *AAPG Bulletin*, *64*, 67–87.

Schröder-Adams, C. J., Herrle, J. O., Selby, D., Quesnel, A., & Froude, G. (2019). Influence of the high Arctic igneous province on the Cenomanian/Turonian boundary interval, Sverdrup Basin, High Canadian Arctic. *Earth and Planetary Science Letters*, *511*, 76–88. https://doi.org/10.1016/j.epsl.2019.01.023

Scopelliti, G., Bellanca, A., Coccioni, R., Luciani, V., Neri, R., Baudin, F., . . . Marcucci, M. (2004). High–resolution geochemical and biotic records of the Tethyan Bonarelli Level (OAE2, latest Cenomanian) from the Calabianca–Guidaloca composite section. *Palaeogeography, Palaeoclimatology, Palaeoecology, 208*(3-4), 293–317. https://doi.org/10.1016/j.palaeo.2004.03.012

Scopelliti, G., Bellanca, A., Neri, R., & Sabatino, N. (2010). Phosphogenesis in the Bonarelli Level from northwestern Sicily, Italy: Petrographic evidence of microbial mediation and related REE behaviour. *Cretaceous Research*, *31*(2), 237–248. https://doi.org/10.1016/j.cretres.2009.11.004

Sepehr, M., & Cosgrove, J. W. (2004). Structural framework of the Zagros fold-thrust belt, Iran. *Marine and Petroleum Geology*, *21*(7), 829–843. https://doi.org/10.1016/j.marpetgeo.2003.07.006

Sepehr, M., & Cosgrove, J. W. (2005). Role of the Kazerun fault zone in the formation and deformation of the Zagros Fold–Thrust belt, Iran. *Tectonic*, *24*.

Setudehnia, A. (1978). The Mesozoic Sequence in SW Iran and Adjacent Areas. *Journal of Petroleum Geology*, *1*(1), 3–42. https://doi.org/10.1111/j.1747-5457.1978.tb00599.x

Sharland, P. R., Archer, R., Casey, D.M., Davis, R. B., Hall, S. H., Heward, A. P., Horbury, A. D., & Simmons, M. D. (2001). *Arabian Plate Sequence Stratigraphy*(pp. 1–371). Bahrain: GeoArabia Special 2, Gulf Petro Link.

Shen, Q. H., Song, B., Xu, H. F., Geng, Y. S., & Shen, K. (2007). Emplacement and metamorphism ages of the Caiyu and Dashan igneous bodies, Yishui County, Shandong Province: Zircon SHRIMP chronology. *Dizhi Lunping*, *50*, 275–284.

Snow, L. J., & Duncan, R. A. (2005). Trace element abundances in the Rock Canyon Anticline, Pueblo, Colorado, marine sedimentary section and their relationship to Caribbean plateau construction and oxygen anoxic event 2. *Paleoceanography*, *20*, PA3005.

Sprovieri, M., Sabatino, N., Pelosi, N., Batenburg, S. J., Coccioni, R., Iavarone, M., & Mazzola, S. (2013). Late Cretaceous orbitally-paced carbon isotope stratigraphy from the Bottaccione Gorge (Italy). *Palaeogeography, Palaeoclimatology, Palaeoecology, 379–380*, 81–94. https://doi.org/10.1016/j.palaeo.2013.04.006

Stoll, H. M., & Schrag, D. P. (2000). High-resolution stable isotope records from the Upper Cretaceous rocks of Italy and Spain: Glacial episodes in a greenhouse planet? *Geological Society of America Bulletin*, *112*(2), 308–319. https://doi.org/10.1130/0016-7606(2000)1122.0.CO;2

Taghavi, A. A., Mørk, A., & Emadi, M. A. (2006). Sequence stratigraphically controlled diagenesis governs reservoir quality in the carbonate Dehluran Field, southwest Iran. *Petroleum Geoscience*, *12*(2), 115–126. https://doi.org/10.1144/1354-079305-672

Tsikos, H., Jenkyns, H. C., Walsworth-Bell, B., Petrizzo, M. R., Forster, A., Kolonic, S., . . . Sinninghe Damste, J. S. (2004). Carbon-isotope stratigraphy recorded by the Cenomanian-Turonian Oceanic Anoxic Event: Correlation and implications based on three localities. *Journal of the Geological Society, 161*(4), 711–719. https://doi.org/10.1144/0016-764903-077

Udgata, D. B. P. (2007). Glauconite as an indicator of sequence stratigraphy package in Lower Paleocene passive-margin shelf succession, Central Alabama. Unpublished Master thesis, Auburn University. 125 p.

van Buchem, F. S. P., Razin, P., Homewood, P. W., Oterdoom, W. H., & Philip, J. (2002). Stratigraphic organization of carbonate ramps and organic-rich intrashelf basins: Natih Formation (middle Cretaceous) of northern Oman. *AAPG Bulletin*, *86*, 21–53.

Vaziri-Moghaddam, H., & Kalanat, B. (2020). Oxygen level, primary productivity, and water turbulence during the OAE2 interval of Zagros Basin (SW Iran): Benthic foraminiferal variations in the carbonate microfacies. *Gondwana Research*, *83*, 1–15. https://doi.org/10.1016/j.gr.2020.01.010

Vink, A. (2004). Calcareous dinoflagellate cysts in South and equatorial Atlantic surface sediments: Diversity, distribution, ecology and potential for palaeoenvironmental reconstruction. *Marine Micropaleontology, 50*(1-2), 43–88. https://doi.org/10.1016/S0377-8398(03)00067-7

Voigt, S., Erbacher, J., Mutterlose, J., Weiss, W., Westerhold, T., Wiese, F., . . . Wonik, T. (2008). The Cenomanian–Turonian of the Wunstorf section (North Germany): Global stratigraphic reference section and new orbital time scale for Oceanic Anoxic Event 2. *Newsletters on Stratigraphy, 43*(1), 65–89. https://doi.org/10.1127/0078-0421/2008/0043-0065

Voigt, S., Friedrich, O., Norris, R. D., & Schoenfeld, J. (2010). Campanian–Maastrichtian carbon isotope stratigraphy: Shelf-ocean correlation between the European shelf sea and the tropical Pacific Ocean. *Newsletters on Stratigraphy*, *44*(1), 57–72. https://doi.org/10.1127/0078-0421/2010/0004

Voigt, S., Gale, A. S., Jung, C., & Jenkyns, H. C. (2012). Global correlation of Upper Campanian–Maastrichtian successions using carbon-isotope stratigraphy: Development of a new Maastrichtian timescale. *Newsletters on Stratigraphy, 45*(1), 25–53. https://doi.org/10.1127/0078-0421/2012/0016

Wefer, G., & Berger, W. H. (1991). Isotope paleontology: Growth and composition of extant calcareous species. *Marine Geology, 100*(1-4), 207–248. https://doi.org/10.1016/0025-3227(91)90234-U

Wendler, J., Gräfe, K. U., & Willems, H. (2002a). Palaeoecology of calcareous dinoflagellate cysts in the mid-Cenomanian Boreal Realm: Implications for the reconstruction of palaeoceanography of the NW European shelf sea. *Cretaceous Research, 23*(2), 213–229. https://doi.org/10.1006/cres.2002.0311

Wendler, J., Gräfe, K. U., & Willems, H. (2002b). Reconstruction of mid-Cenomanian orbitally forced palaeoenvironmental changes based on calcareous dinoflagellate cysts. *Palaeogeography, Palaeoclimatology, Palaeoecology, 179*(1-2), 19–41. https://doi.org/10.1016/S0031-0182(01)00366-2

Wendler, I., Zonneveld, K. A. F., & Willems, H. (2002c). Production of calcareous dinoflagellate cysts in response to monsoon forcing off Somalia: A sediment trap study. *Marine Micropaleontology, 46*(1-2), 1–11. https://doi.org/10.1016/S0377-8398(02)00049-X

Wendler, I., Wendler, J., Gräfe, K. U., Lehmann, J., & Willems, H. (2009). Turonian to Santonian carbon isotope data from the Tethys Himalaya, southern Tibet. *Cretaceous Research, 30*(4), 961–979. https://doi.org/10.1016/j.cretres.2009.02.010

Wendler, I. (2013). A critical evaluation of carbon isotope stratigraphy and biostratigraphic implications for Late Cretaceous global correlation. *Earth-Science Reviews, 126*, 116–146. https://doi.org/10.1016/j.earscirev.2013.08.003

Wendler, I., Wendler, J. E., & Clarke, L. J. (2016). Sea-level reconstruction for Turonian sediments from Tanzania based on integration of sedimentology, microfacies, geochemistry and micropaleontology. *Palaeogeography, Palaeoclimatology, Palaeoecology, 441*, 528–564. https://doi.org/10.1016/j.palaeo.2015.08.013

Wilmsen, M. (2003). Sequence stratigraphy and paleoceanography of the Cenomanian Stage in northern Germany. *Cretaceous Research, 24*(5), 525–568. https://doi.org/10.1016/S0195-6671(03)00069-7

Wilson, J. L. (1975). *Carbonate Facies in Geologic History* (pp. 1–471). Heidelberg: Springer-Verlag. https://doi.org/10.1007/978-1-4612-6383-8

Wynd, J. G. (1965). Biofacies of the Iranian consortium-agreement area. Iranian Oil Operating Companies Report 1082. Unpublished.

Ziegler, M. A. (2001). Late Permian to Holocene Paleofacies Evolution of the Arabian Plate and its Hydrocarbon Occurrences. *GeoArabia, 6*(3), 445–504. https://doi.org/10.2113/geoarabia0603445

Manuscript received: June 19, 2024
Revisions requested: October 07, 2024
Accepted: June 17, 2025